Article:
Gong, Y., Morina, A. orcid.org/0000-0001-8868-2664, Wang, C. orcid.org/0000-0002-4301-3974 et al. (5 more authors) (2022) Experimental and numerical study on wear characteristics of steel surfaces involving the tribochemistry of a fully formulated oil. Part I: Experiments. Tribology International, 176. 107888. ISSN 0301-679X

https://doi.org/10.1016/j.triboint.2022.107888

Experimental and Numerical Study on Wear Characteristics of Steel Surfaces Involving the Tribochemistry of a Fully Formulated Oil Part I: Experiments

Yajing Gong[a*], Ardian Morina[a*], Chun Wang[a], Yuechang Wang[a], Yukio Tamura[b], Akihito Ishihara[b], Ali Ghanbarzadeh[a], Anne Neville[a]

* Corresponding authors: artemisgong@hotmail.com (Yajing Gong); a.morina@leeds.ac.uk (Ardian Morina)
a Institute of Functional Surfaces, School of Mechanical Engineering, University of Leeds, Leeds, LS2 9JT, United Kingdom
b Manufacturing Engineering Development Centre, Production Division, Komatsu Ltd., Osaka 573-1011, Japan

Abstract:

This paper studied a fully formulated oil (FFO) in the hydraulic piston pump, containing mainly zinc dialkyldithiophosphate (ZDDP), detergents, and dispersants. The results of tribo-tests show that the antiwear characteristics are different when using FFO compared to using a single additive oil such as base oil + ZDDP. A two-phase temperature-dependent wear trend was found when FFO is used. Phase (I) is in the low-temperature range, where wear increases with increasing tribofilm thickness and temperature. Phase (II) is in the high-temperature range where the tribofilm thickness increases but wear decreases as the temperature increases. Raman spectroscopy and X-ray photoelectron spectroscopy (XPS) analysis of the tribofilm show that the most temperature-dependent compositions are phosphate and iron sulphides, where the signal intensity of phosphates increases, but that of sulphides decreases when the temperature increases. It indicates that the participation of detergent and ZDDP in the tribofilm formation increases at low and high temperatures, respectively. However, no signal shows the dispersant participating in the tribofilm formation. A hypothesis of mechanisms of reaction priority or enhanced competition among different additives at different temperatures is proposed from the iron loss perspective to explain the two-phase temperature-dependent wear mechanism. This study also provides the experimental basis for the wear modelling involving the tribochemistry of FFO in Part (II) of the research series.

Keywords: Fully Formulated Oil; Wear; ZDDP; Detergent

1 Introduction

Wear is an important reason for affecting machinery life and increasing maintenance costs in the industry [1, 2]. Mild wear can lead to reduced machine efficiency, while severe wear can lead directly to the failure of the machine. Lubrication is one of the commonly used methods to reduce wear. However, it is difficult to prevent the wear between relatively moving components/parts, such as piston/cylinder or gear pairs, due to lubricant

starvation caused by mechanical vibration or fit errors. In the hydraulic system, hydraulic fluids perform the functions of lubrication and heat dissipation like conventional lubricants and energy transmission [3]. This requires the hydraulic lubricants to have antiwear behaviour and stable performances in other aspects, such as cleaning the contaminants and preventing oxidation.

Fully formulated oils (FFO) contain various additives (such as antiwear additives, detergents, dispersants, and antioxidants), which are added to the base oil (such as mineral oil and synthetic oil) with a specific concentration. They are used to fulfil the multifunctionality in applications. However, since FFOs have high levels of chemical complexity, it is challenging to study the effect of detailed compositions of FFO on antiwear performance and wear prediction. Decades of research on each kind of additive or its combinations have shown that additives' type, concentration, acidity, and alkalinity affect their antiwear behaviours. The same additive may perform differently under different working conditions [4-9].

Zinc dialkyldithiophosphate (ZDDP) is a widely used antiwear additive. Film formation is a significant function of ZDDP. Many studies showed that tribofilm only formed within the rubbing tracks [10, 11] and that the tribofilm thickness stabilises over 50~150 nm on steel surfaces [10, 12, 13]. The formation rate of tribofilm increases with the increase in temperature and concentration of ZDDP [12]. The main compositions from the tribofilm surface to the substrate are alkylphosphate precipitates, polyphosphate (Zn), phosphate (Zn/Fe), and Fe/Zn sulphides near the substrate [14]. It was found that the antiwear effect of ZDDP is mainly derived from the formation of phosphates [9].

The primary function of detergents is to clean the acidic substances in the lubricant, so it is usually alkaline or neutral. Over-based calcium sulphonate is a commonly used detergent that can form a boundary film on the steel surface that contains mainly calcium carbonate and/or CaO [4, 6, 15-18]. It has been found that the tribofilm formed by the overbased calcium sulphonate detergent can grow to 160 nm in 2 hours [19], but its formation process is different from ZDDP, which does not require much iron to be involved [15]. Although the overbased calcium sulphonate detergent was found to have antiwear and anti-scuffing properties [5, 15, 20-23], it was reported when combined with ZDDP to have an antagonistic effect on the antiwear performance of ZDDP [24-28].

The primary role of dispersants is to keep insoluble substances suspended in oil and avoid deposition on the surface. It usually contains a higher molecular weight that can help maintain the oil viscosity. Most dispersants are considered to have little effect on wear or friction [29]. However, some studies have shown that dispersants and ZDDP have antagonistic effects on wear reduction due to complexation [8, 30-32]. In addition, the dispersant may adsorb or react with metal surfaces [33-35] or dissolve the existing ZDDP tribofilm [8], which will also reduce the effectiveness of the antiwear properties of ZDDP.

The antiwear performances of single additive or combinations of different additives have been well studied for many years. However, it still cannot answer the performance of the FFO as a whole, even if the type, concentration, and other information of additives contained in the FFO are known. In recent years, more experimental studies have used FFOs to study antiwear performance [36-39]. One aspect of FFO studies is to evaluate the performance of the additives contained therein on different material surfaces. On the other hand, the interaction between multiple additives can be more abundantly and directly understood by comparing their combined behaviour with that of a single additive. Experimental testing is the primary method for studying the antiwear performance of FFOs. However, experimentally understanding the wear mechanism is not enough for FFO users to monitor the machine's service life. Advanced modelling and numerical simulation techniques are also necessary to quantify the wear process and predict failures.

Therefore, this work studied a commercial FFO used in the hydraulic system, containing the antiwear additive ZDDP, detergents overbased calcium sulphonate and phenate, and the dispersant succinimide. A two-part series of papers are organised to report the experimental findings, and theoretical modelling works. This paper, the first part, presents an experimental study on the wear mechanism involving the FFO and its tribochemistry under different temperatures. The experimental results are then used for the modelling work to establish the theory and to simulate the main tribological phenomena such as tribofilm growth and wear evolution, which will be discussed in Part (II) of the research series.

2 Methodology

2.1 MTM-SLIM

Tribotests are conducted by Mini Traction Machine with the Spacer Layer Imaging Method (MTM-SLIM, PCS Instruments, UK), as shown in Fig. 1. The MTM is a tribometer with a ball-on-disc configuration (see Fig. 1a), which allows the rotation speed of the ball and disc to be adjusted independently to achieve different sliding/rolling conditions. The SLIM is an external component of the MTM for testing the *in-situ* growth process of the tribofilm and analysing the thickness after the test, which has been widely used in many studies of ZDDP tribofilm [10, 12, 40-46]. The main principle is shown in Fig. 1b. Through a lens (consisting of a glass flat, a thin semi-reflective chromium layer and a silica spacer layer), a white light source and its reflected light from the steel surface produce an interference image of the tribofilm, which is captured by a colour camera and microcomputer. After the test, the RGB colour of each pixel in the image is analysed by offline software, and the tribofilm thickness is calculated automatically.

The ball has a diameter of 3/4 inch (~19 mm) with a roughness of 20 nm (Ra), and the disc has a diameter of 46 mm with a roughness of 10 nm. The material of both the ball and the disc is AISI52100 steel. The lubricant is a hydraulic FFO (provided by Komatsu Ltd., Japan), and its specifications are listed in Table 1. The base oil in the FFO is a low viscosity mineral oil with a kinetic viscosity of 36 cSt at 40 °C and 5.9 cSt at 100 °C. The main

additives are a mixture of primary and secondary ZDDPs, overbased calcium sulphonate, overbased calcium phenate, and succinimide.

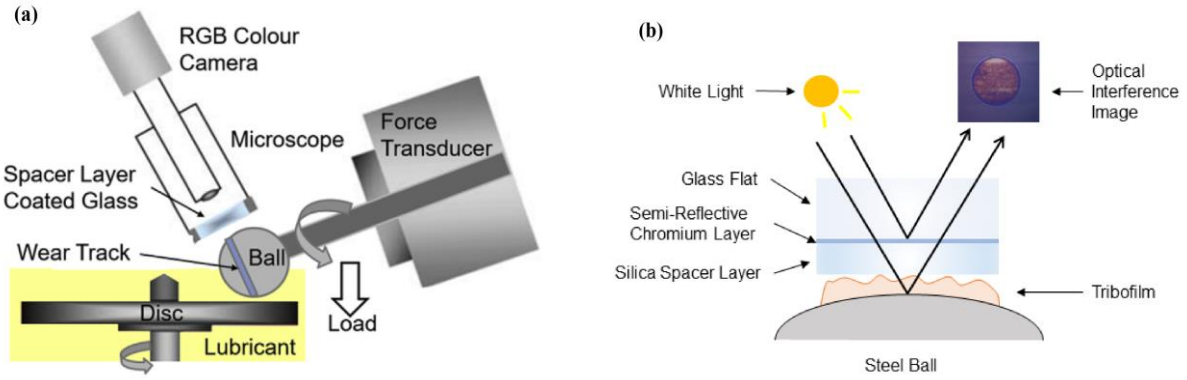

Fig. 1 a) Schematic diagram of MTM-SLIM [46]; b) SLIM principle.

Table 1 Specification of the FFO.

Fully Formulated Oil	**Types**
Base Oil	Mineral Oil (Kinetic viscosity: 36 cSt at 40 °C, 5.9 cSt at 100 °C)
Antiwear Additive	Primary and Secondary ZDDP (0.08 wt.% P)
Detergents	Over-based calcium sulphonate/phenate (0.38 wt.% Ca)
Dispersant	Succinimide

Considering the application of hydraulic piston pumps, the test conditions are designed in Table 2. According to the ISO 6743-4 hydraulic fluid classification system [47], the operating temperature range of mineral oils with antiwear additives is about -10 °C ~ 90 °C. However, for some high-temperature applications, the upper-temperature limit can reach 120 °C [48], so the main test temperatures in this study are 60, 80, 100, and 120 °C. The load is 60 N to have an equivalent maximum Hertzian pressure of 1.2 GPa. The entrainment speed is 100 mm/s, and the slide-to-roll ratio (SRR) is 150 %. The tests are designed in a boundary lubrication regime. The maximum test duration is 6 hours, and there are different test intervals for wear measurements.

Table 2 Working conditions for MTM-SLIM tests

Traction Mode	
Temperatures	60, 80 100 and 120 °C
Load	60 N
Entrainment Speed	100 mm/s
SRR	150 %
Duration	6h with different intervals

Before testing, heptane is first used to clean the antirust oil and dust on the surface of the samples with soft tissue. Then, the samples are immersed in an acetone solution and cleaned in an ultrasonic bath for 30 mins. Finally, the samples are rinsed with methanol and dried naturally. After the MTM tests, the samples are rinsed with heptane to remove the remained lubricants on the surface and then dried naturally.

2.2 White Light Interferometry

The wear measurements were carried out by white light interferometry (NPFLEX^{TM}, Bruker, UK/USA). Since the tribofilm generated by ZDDP contains phosphate, which has light transmittance and interferes with white light interference measurement [49], the tribofilm must be removed before wear measurement. The 0.05 mol/L ethylenediaminetetraacetic (EDTA) solution was used in many studies to remove tribofilm formed by ZDDP [41, 49] and over-based calcium sulphonate detergent [19]. Thus, it is considered to apply to the tribofilm formed by FFO containing these two film-forming additives.

Wear measurement was carried out with a total magnification of 10× with a measurement area of 400×600 μm^2. The results are processed by the built-in Vision64® software, which allows the wear volume in the measured area to be calculated directly. Since tests were run at a high SRR of 150 %, the disc sliding distance is six times higher than the ball for the same test duration. The length of the disc wear track is approximately three times that of the ball, so the disc wears more than the ball. Fig. 2 shows the examples of wear results on the ball and on the disc, also indicating that the wear on the ball (Fig. 2a) is very small and hard to measure at the maximum test time, so only the wear results on the discs are discussed in the following sections.

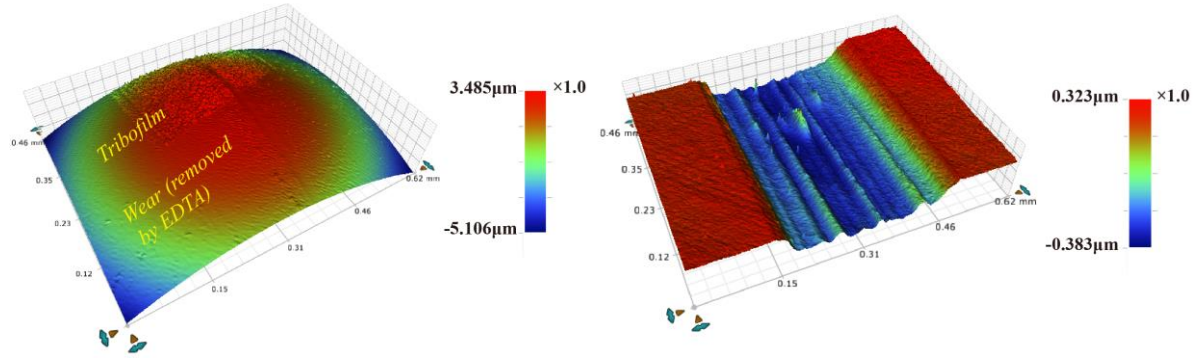

Fig. 2 The 3D images of worn surfaces on (a) the steel ball and (b) the steel disc after 6-hour testing at 100 °C, captured by NPFLEX with the magnification of 10X.

2.3 Raman Spectroscopy

Raman spectroscopy (Renishaw inVia, UK) measures mainly sulphides and phosphates in the tribofilm. The laser with the wavelength of 488 nm is chosen, and its maximum energy is 10 mW. The laser intensity is 50 %. The acquisition range is 150 cm^{-1}~1600 cm^{-1}, and the acquisition time is 30 seconds. There are 1~2 areas of the tribofilm selected randomly on the ball and disc, and 22 spectra are analysed for one test condition. The one with the strongest signal is chosen for comparison.

After obtaining the Raman spectrum, the baseline of the raw data is removed first. Then, a mixed Gaussian/Lorentzian method is used to fit the peaks to obtain the information of frequency, intensity and full width at half maximum (FWHM).

2.4 X-ray Photoelectron Spectroscopy (XPS)

The XPS instrument used in this work is the PHI5000 Versa Probe II^{TM} (ULVAC-PHI Inc., Japan/USA). Conventional XPS analysis can provide the chemical structure at the top surface of 5~10 nm [26]. However, in analogy with the tribofilm formed by ZDDP, the chemical compositions in the tribofilm should be different along with depth, so the depth profiling with the high-resolution XPS spectral analysis is used to analyse the key elements and compounds in the tribofilm from the top surface to the substrate. An Al Kα monochromatic source is used at 15 kV and 50 W with a step energy of 1486.6 eV. The test area is in the centre of the tribofilm and is approximately 200 µm in diameter. The Ar ion sputtering is applied for etching the specimens with 4 kV and 20 mA energy. The high-resolution C1s, N1s, O1s, P2p, S2p, Ca2p, Fe2p, and Zn2p3 spectra are collected at a pass energy of 23.5eV with an acquisition step size of 0.1eV. The etching rate is 18.175nm/mins as the reference of SiO_2. The maximum etching depth is about 120 nm.

The post-processing process of XPS data is performed using CasaXPS software. The Shirley-Sherwood iterative method is used for background subtraction, and Gaussian and Lorentzian functions are applied for curve-fitting

the peaks. For 2p spectra of elements P, S, and Ca, due to the splitting of the spin orbits, a doublet with an area ratio of 2:1 is set in the peak fitting.

3 Tribological Results

3.1 Tribofilm Formation

The evolution of the FFO tribofilm thickness at different temperatures is shown in Fig. 3. The growth curves of FFO tribofilm (Fig. 3a) can be divided into two phases: (I) growth phase and (II) stable phase. In the growth phase, the tribofilm thickness increases rapidly at the beginning. The growth rate primarily increases with an increase in temperature. In the stable phase, the tribofilm thickness reaches a dynamic balance that is primarily unchanged at each temperature. When the temperature rises, the average balanced thickness increases, which can grow to about 120 nm at 120 °C. The growth process of FFO tribofilm is similar to that of tribofilm formed by ZDDP with a higher carbon length [12, 41]. However, it can also be noted that the growth rate of the FFO tribofilm decreased and then increased between 15 mins and 60 mins of the test time, especially at 80 °C and 100 °C. The interferometry images of the tribofilm captured by SLIM exhibit the morphology of the tribofilm at different test durations, as shown in Fig. 3b. The tribofilm distribution appears to be more uneven in the contact at lower temperatures.

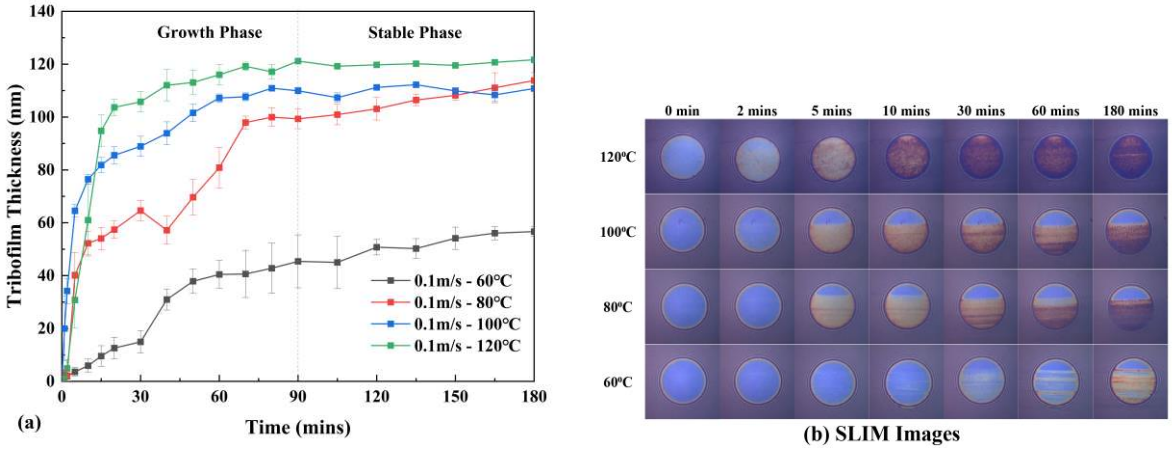

Fig. 3 MTM-SLIM results of (a) FFO tribofilm growth and (b) SLIM images at different temperatures (60, 80, 100 and 120 °C).

3.2 Friction Coefficient

Fig. 4 shows the friction coefficients corresponding to the FFO tribofilm growth process at different temperatures. As shown in Fig. 4a, all the friction coefficients in the steady-state phase increase compared to the initial values at the four tested temperatures. However, the evolution process is varied from temperature to temperature. At 60 °C, the friction coefficient experiences a slow increase and then reaches a steady state. Its growth rate and the value in the steady-state phase are the lowest of all the temperatures tested. The changes in friction coefficient are relatively similar at 80 °C and 100 °C, but the friction coefficient at 100 °C is overall

slightly higher than that at 80 °C. During the first 15 mins of the test, it increases rapidly. After a 'reduction and regrowth' process, a plateau is reached. Comparing the growth curve of the tribofilm at the same temperature in Fig. 3a, the growth rate of the tribofilm has a similar variation. The friction coefficient at 120 °C also increases rapidly before reaching a stable value, where the increase rate is lower than that at 80 °C and 100 °C. However, the friction coefficient at 120 °C in the steady-state phase has the maximum value.

The average steady-state friction coefficient and corresponding average tribofilm thickness after 90 mins of testing at each temperature are calculated, as illustrated in Fig. 4b. With the increase in temperature, the friction coefficient and the tribofilm thickness in the steady-state phase increase with a similar trend.

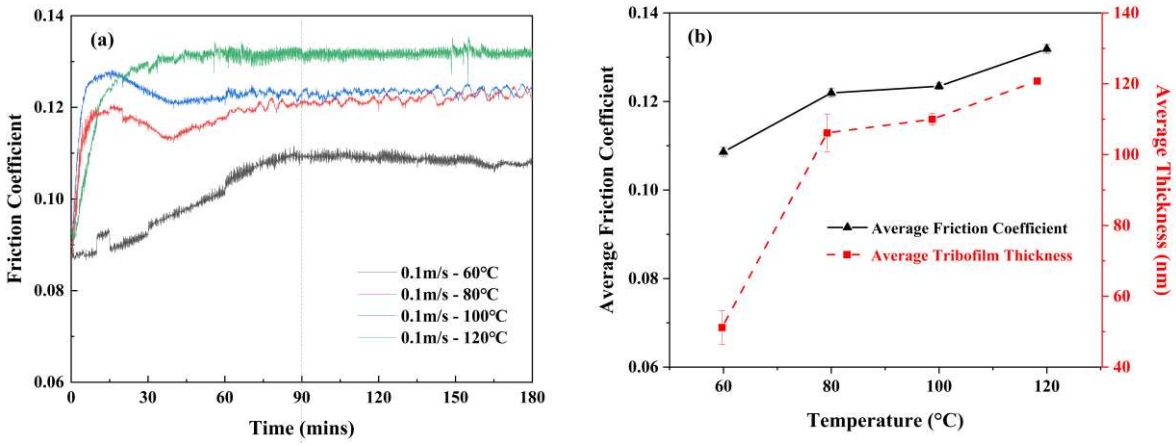

Fig. 4 MTM-SLIM results of (a) friction coefficients at different temperatures (60, 80, 100 and 120 °C) and (b) average friction coefficient at the stable phase compared with average thickness at each temperature.

Some researchers have shown that different compositions in the tribofilm may lead to differences in the friction coefficients. For example, the formation of ZDDP tribofilm can increase the friction coefficient on the steel surface [11, 50], while the formation of iron sulphide may reduce the friction coefficient [51, 52]. Therefore, the changes in friction coefficients indicate that the growth process and chemical composition of tribofilms formed at different temperatures may differ.

3.3 Wear Results

Fig. 5 shows the wear results at different temperatures. Unlike the *in-situ* tests of tribofilm thickness, the wear results are only measured after the tribotests are finished, so the increase in wear may be discontinuous at the same temperature. The wear evolution can be seen in Fig. 5a, where the highest wear occurs at 80 °C, but the results at 100 °C are very close. When the temperature increases to 120 °C, the expected wear reduction is identified due to the antiwear performance of the additives. Unexpectedly, the lowest wear occurs at 60 °C. As temperature increases from 60 °C to 80 °C, wear and tribofilm thickness increase, which does not seem to reflect

the protective effect of the tribofilm on the surface. Thus, the reasons for the wear trend in this lower temperature range must be further explored.

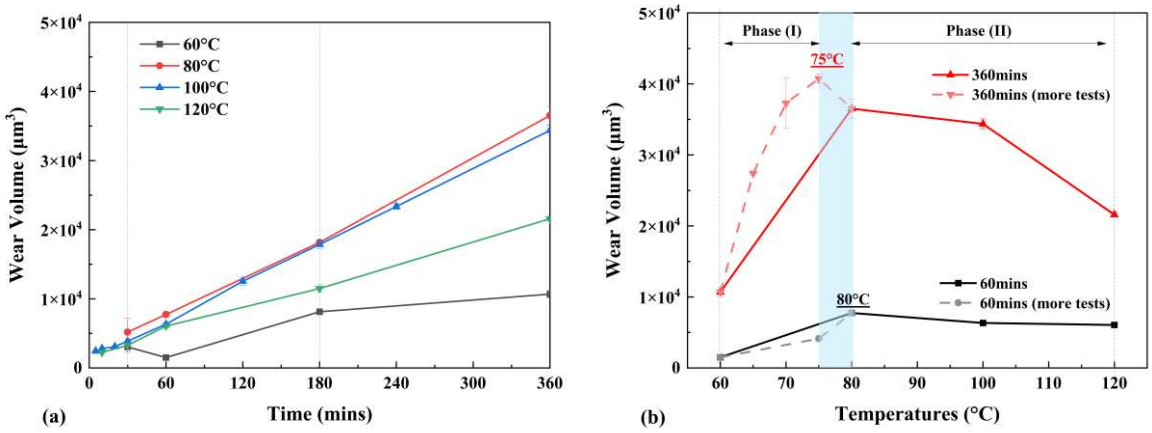

Fig. 5 Wear measurements on steel discs by NPFLEX at different temperatures: (a) evolution of wear volume; (b) wear volume as the function of the temperature at the test durations of 60 mins and 360 mins.

In order to analyse the correlation between wear and temperature more clearly, the wear data in the test duration of 60 mins and 360 mins at different temperatures are extracted in Fig. 5b from Fig. 5a. More tests (65, 70, 75 °C for 360 mins and 75 °C for 60 mins) are conducted to confirm the wear trend in the temperature range of 60~80 °C (see the dash lines in Fig. 5b). For the tests at 60 mins and 360 mins, the maximum wear occurs at 80 °C and 75 °C, respectively. It is speculated that the change of the wear mechanism of FFO may happen around 75/80 °C. As the difference between the two temperatures is minor, to simplify the description, the subsequent description uses 80 °C as the threshold to divide the wear trend of FFO. Hence, it can be summarised that the wear trend when using FFO is two-phase temperature-dependent, that is, phase (I): in the low-temperature range of 60~80 °C, wear increases with the increase in temperature; and phase (II): in the high-temperature range of 80~120 °C, when the temperature rises, the wear decreases.

Considering the viscosity of the lubricants decreases with increasing temperature, the lower wear at 60 °C may be because it is not entirely in the boundary lubrication regime, so the fluid carries part of the applied load between asperities, resulting in the reduction of wear and tribofilm formation. To further investigate the effect of this factor, the author conducted a set of experiments with a lower λ ratio by only reducing entrainment speed from 0.1 m/s to 0.01 m/s. The wear results at a lower λ ratio still exhibit the same two-phase trend with temperature (results are shown in Supplementary Material for brevity), so the influence of viscosity can be eliminated. Based on these results, it can be suggested that the change of wear mechanism as a function of testing temperature could be mainly caused by different chemical compositions or the formation process of the tribofilm in the wear track.

4 Chemical Analysis

4.1 Raman Analysis

Since FFO contains ZDDP and overbased calcium sulphonate detergent, it is speculated that phosphate and sulphide are mainly present in the tribofilm. Raman spectroscopy is used for analysis, in which the Raman shift ranges of 200~500 cm^{-1} and 800~1200 cm^{-1} are selected as the spectral analysis sections for sulphide [53-59] and phosphate [60-62], respectively.

Fig. 6(a~d) shows the sulphide sections for the tribofilm after 3 hours of testing at different temperatures. The possible sulphides in tribofilm are likely to be FeS/FeS_2, ZnS, and CaS. At all tested temperatures, the Raman spectra are mainly composed of a strong peak at 374±2 cm^{-1} accompanied by a small peak at 337±3 cm^{-1} and a weak peak at 418±3 cm^{-1}, which are consistent with the reference spectra of pyrite-FeS_2 [53]. In addition, the weak peaks at 319 cm^{-1} and 315 cm^{-1} appear at 100 °C and 120 °C, respectively, which may be attributed to the marcasite structure of FeS_2 [54]. When the temperature increases, iron sulphide's signal intensity significantly reduces. However, the typical peak for ZnS is around 349 cm^{-1} [55, 56], which cannot be separated from the Raman results. Furthermore, the primary Raman shifts for Ca-S at 285 cm^{-1}, 215 cm^{-1}, 185 cm^{-1}, and 160 cm^{-1} [57] are not found within the measurement range of the Raman analysis. Compared to the Raman results for the ZDDP tribofilm in Ref.[58], the peaks detected for sulphides are likely to be 386 cm^{-1} for Fe-S and 351 cm^{-1} for Zn-S. However, for an engine oil containing ZDDP and calcium S-based detergent, the peak for FeS_2 was detected [59]. Thus, the iron sulphides detected in FFO tribofilm are mainly the product of interaction between ZDDP and detergent.

Fig. 6(e~h) shows the phosphate section for the tribofilm after testing for 3 hours at different temperatures. The possible phosphates in the tribofilm are probably Ca/Zn/Fe phosphate. There are mainly two strong peaks and one weak peak. The first peak is at 952±1cm^{-1}, which can be assigned to ν_1-PO_4 with the symmetrical stretching mode [61]. It is more likely to be assigned to calcium phosphate due to the presence of detergents, but there may be a small amount of zinc phosphate and/or iron phosphate. The second peak is at 1080±1 cm^{-1}, which can be assigned to ν_1-CO_3 with the symmetrical stretching mode or ν_3-PO_4 with the antisymmetric stretching mode [61, 62]. The latter has a lower Raman shift, and its signal intensity usually is not higher than the peak ν_1-PO_4. Therefore, it is mainly attributed to the presence of calcium carbonate when the temperature is lower than 100 °C. Between the two peaks, weak peaks at 997±2 cm^{-1} and 1041±4 cm^{-1} can be assigned to other stretching modes of P-O from PO_4 or PO_3 group [60-62].

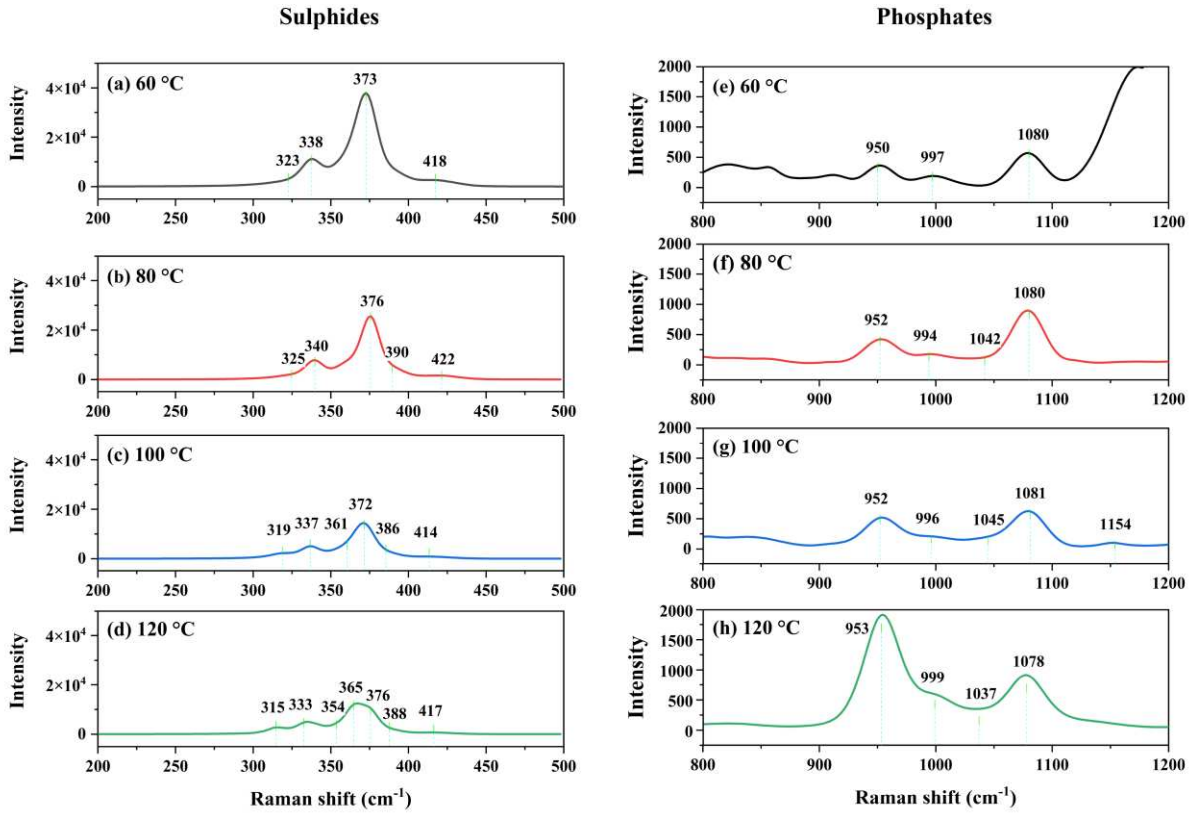

Fig. 6 Raman spectra of sulphide (a-d) and phosphate (e-h) in the tribofilms after testing for 3 hours at different temperatures (a,e) 60 °C, (b,f) 80 °C, (c,g) 100 °C, and (d,h) 120 °C.

It can be inferred from Raman analysis that the FFO tribofilm contains iron sulphide, calcium phosphate, and calcium carbonate. With the increase in temperature, the peak intensity of iron sulphide decreases, but that of phosphate increases.

4.2 XPS Depth Profiling Analysis

XPS depth profiling analysis combined with high-resolution elemental spectra is used to determine the chemical compositions of FFO tribofilm along the depth direction at different temperatures. The elements C, O, N, P, S, Ca, Fe, and Zn, are chosen for analysis. Since there is no N signal for all tested samples, N spectra are ignored. The XPS signals of C1s, O1s, P2p, S2p, Ca2p, and Zn2p3 at four temperatures are shown in Fig. 7 ~ Fig. 12, respectively.

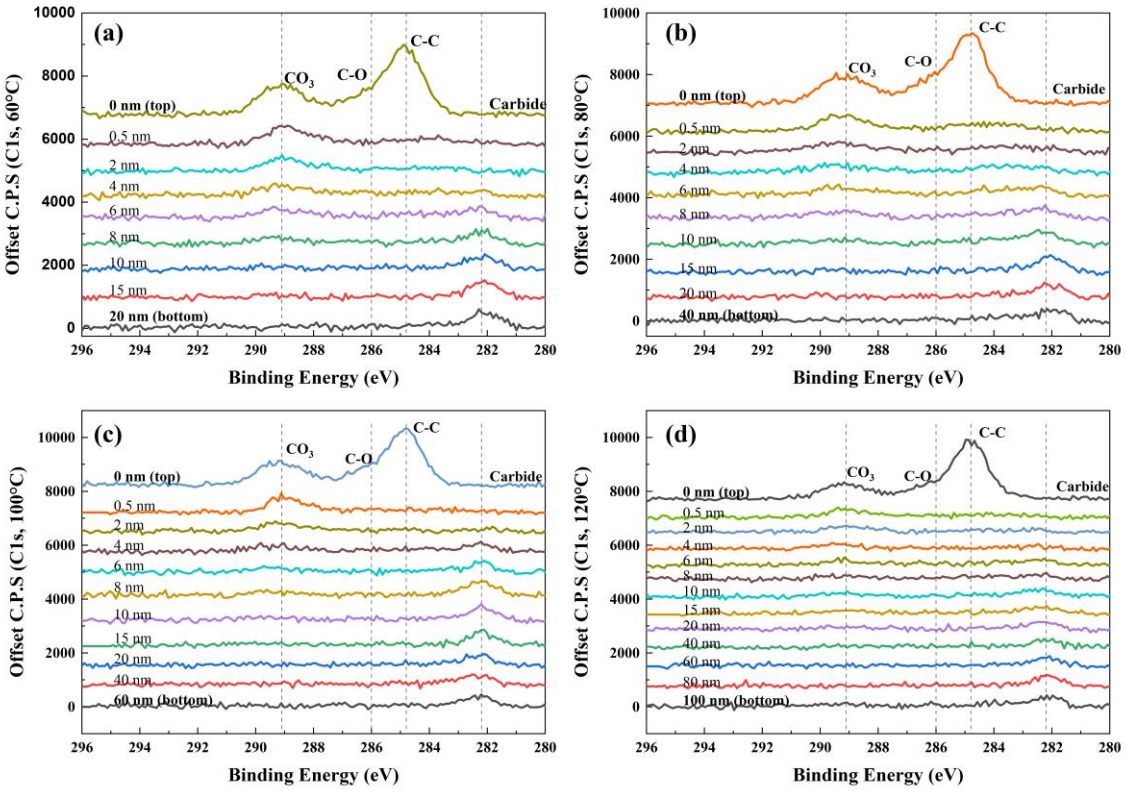

Fig. 7 The C1s spectra of XPS depth profiling of tribofilm on the disc after the 3-hour test at different temperatures (a) 60 °C, (b) 80 °C, (c)100 °C, and (d) 120 °C.

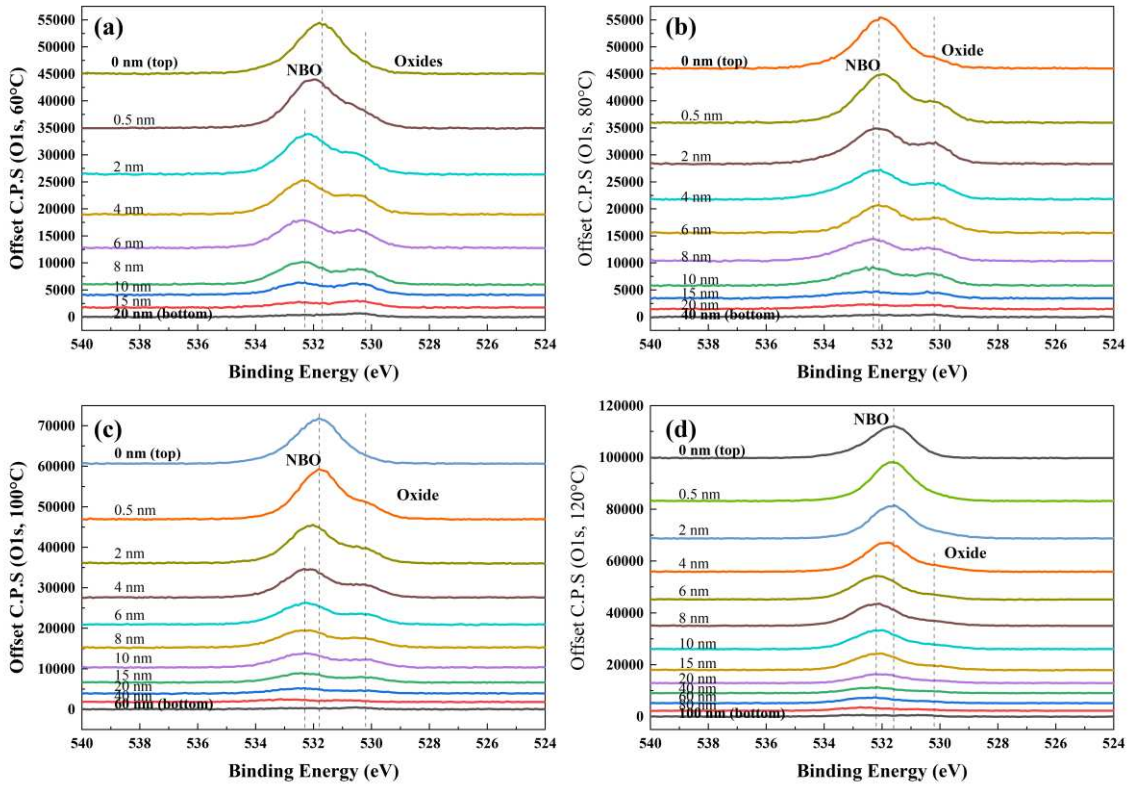

Fig. 8 The O1s spectra of XPS depth profiling of tribofilm on the disc after the 3-hour test at different temperatures (a) 60 °C, (b) 80 °C, (c)100 °C, and (d) 120 °C.

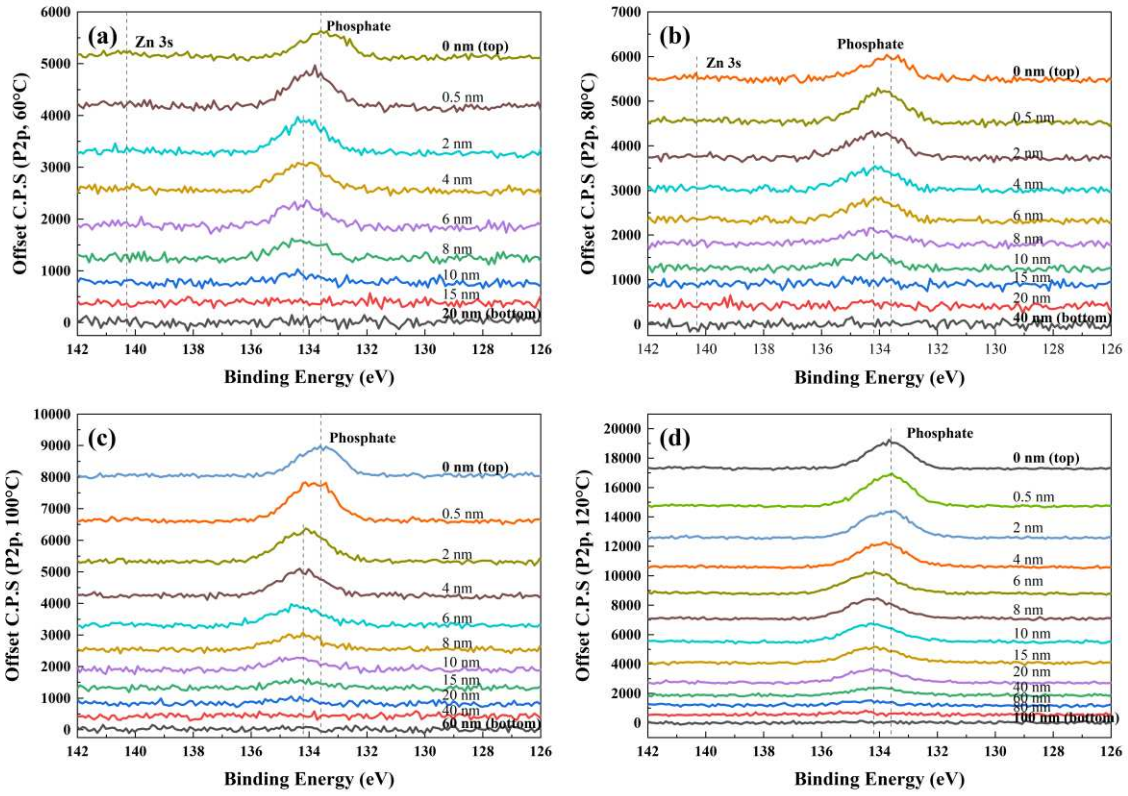

Fig. 9 The P2p spectra of XPS depth profiling of tribofilm on the disc after the 3-hour test at different temperatures (a) 60 °C, (b) 80 °C, (c)100 °C, and (d) 120 °C.

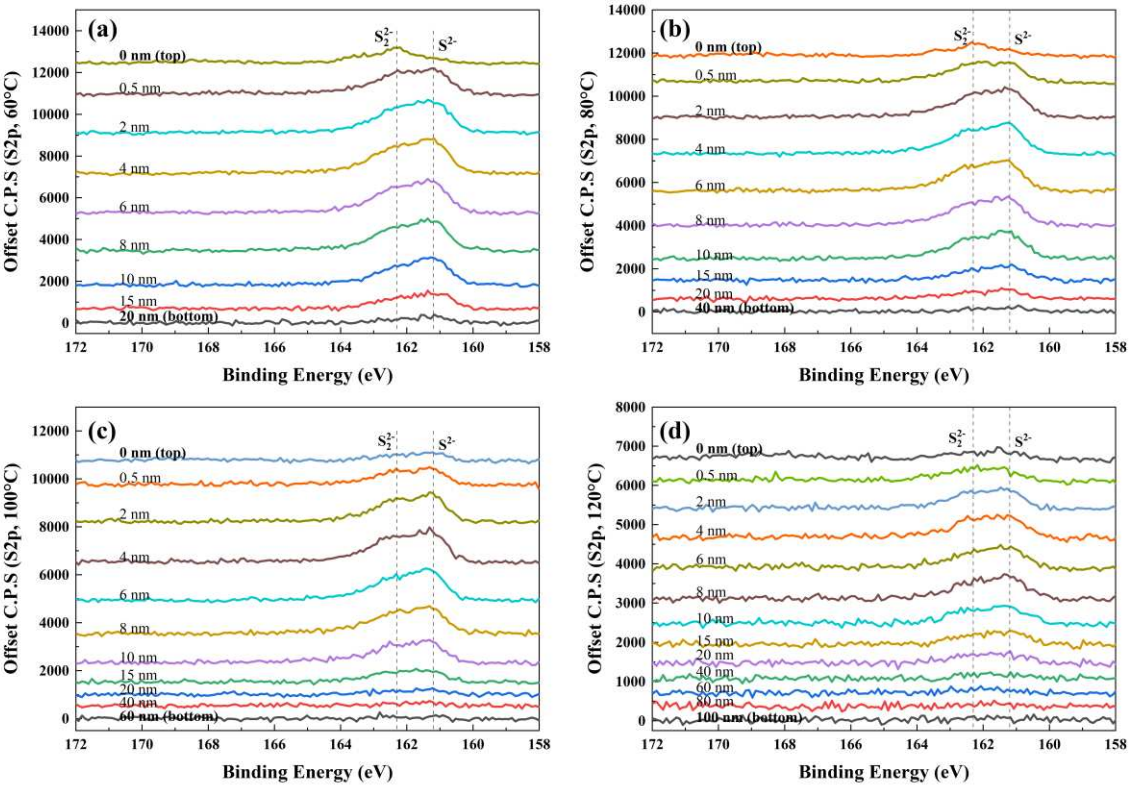

Fig. 10 The S2p spectra of XPS depth profiling of tribofilm on the disc after the 3-hour test at different temperatures (a) 60 °C, (b) 80 °C, (c)100 °C, and (d) 120 °C.

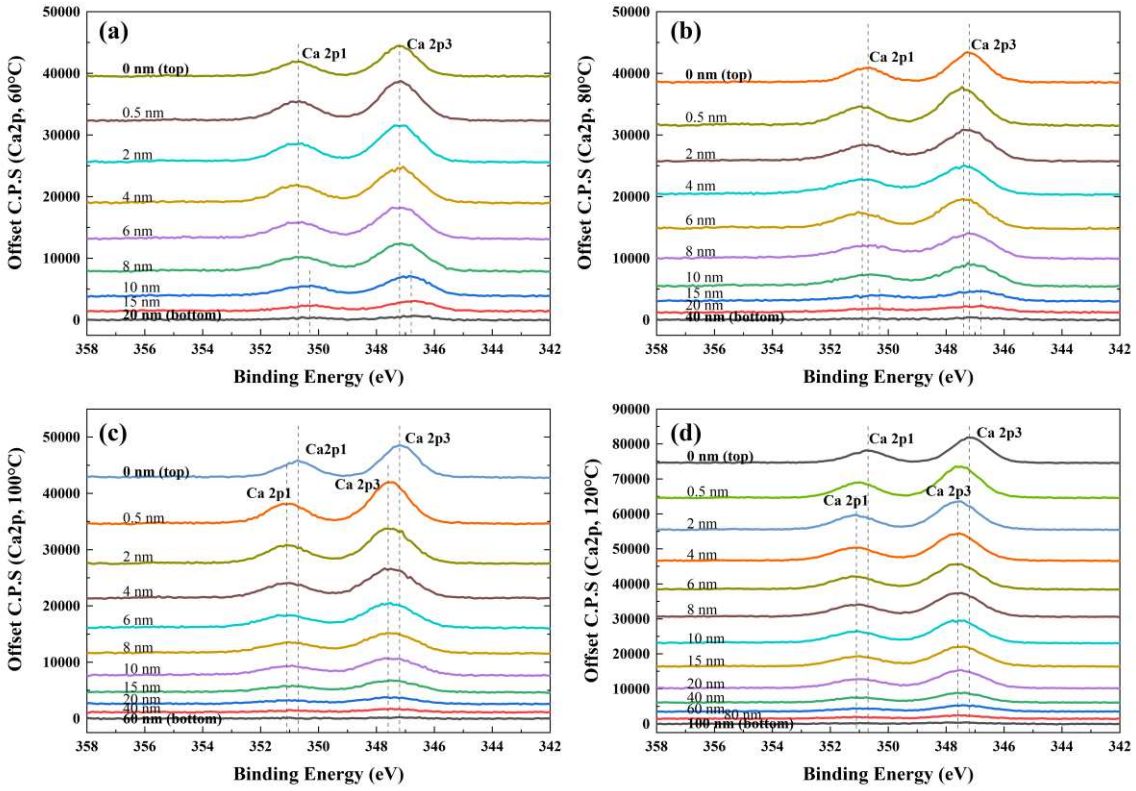

Fig. 11 The Ca2p spectra of XPS depth profiling of tribofilm on the disc after the 3-hour test at different temperatures (a) 60 °C, (b) 80 °C, (c)100 °C, and (d) 120 °C.

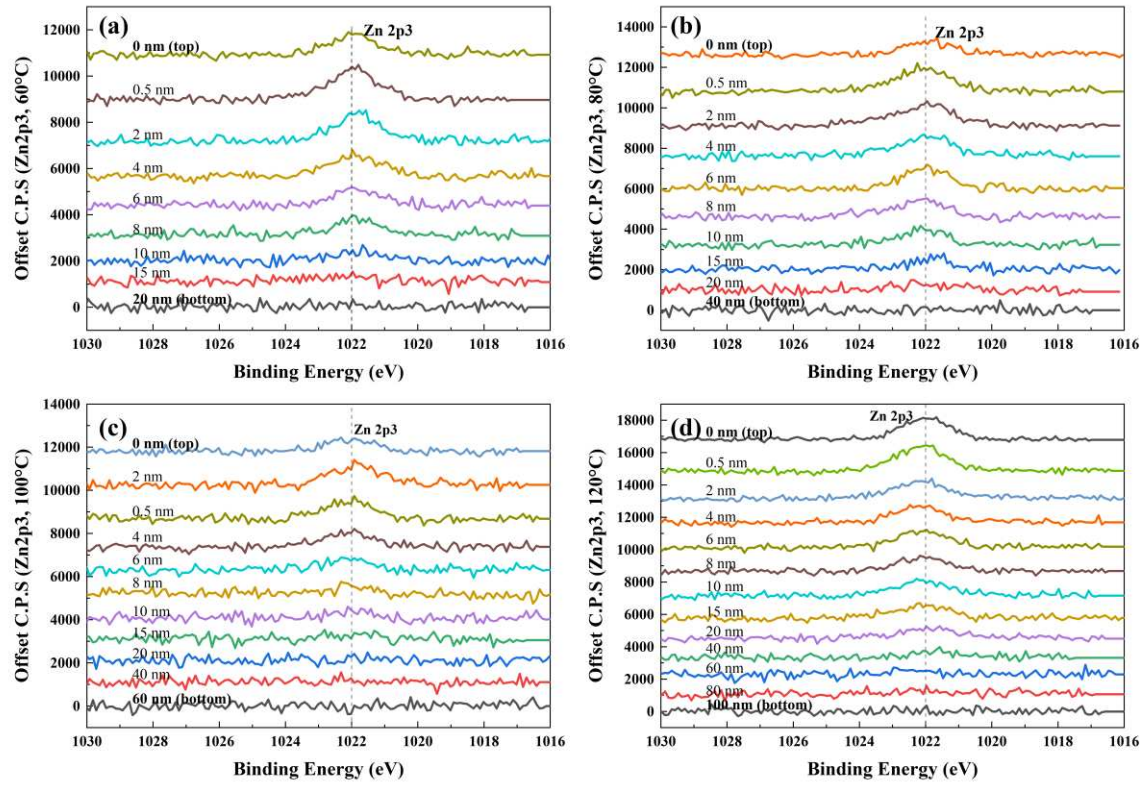

Fig. 12 The Zn2p3 spectra of XPS depth profiling of tribofilm on the disc after the 3-hour test at different temperatures (a) 60 °C, (b) 80 °C, (c)100 °C, and (d) 120 °C

Fig. 7 shows the variation of the C1s spectra with etching depths at four temperatures. Two separate peaks can be observed on the surface, 284.8 eV and 289.1 eV, which are attributed to the organic carbon bond (C-C, C-H) and the carbonate (CO_3) in calcium carbonate [6, 63, 64], respectively. Another peak hidden at 286 eV is the C-O bond in carbonate [65]. With the increased etching depth, another peak at 282.2 eV appeared, which may be assigned to the peak of carbide [66, 67], indicating that the depth reached the substrate.

The O1s spectra in Fig. 8 show the two prominent peaks at 530.2 eV and 531.7 eV, assigned to metal oxide [63] and NBO (non-bridging oxygen) in phosphate, carbonate, or sulphate [6, 63-65, 68], respectively. As the temperature increases, the peak intensity of the metal oxide decreases, indicating that there is more tribofilm formed on the surface, which is consistent with the experimental results of tribofilm thickness. The NBO peak moves to 532.1 eV in the middle layer of the tribofilm. These results may be due to an overlap with a BO (bridging oxygen, such as P-O-P) peak, which has higher binding energy than the NBO peak [45, 63].

The P2p spectra at different temperatures are shown in Fig. 9. Using an area ratio of 2:1 to split the peak due to the splitting of the 2p orbital, the binding energy of the P2p3 peak is approximately 133.2~133.8eV, which is attributed to the phosphate. On the surface of the tribofilm, the binding energy of this peak is lower, and as the etching depth increases, the peak shifts to the higher binding energy. The increase in the binding energy of the P2p3 (phosphate) peak may be due to the change in metal cations such as Ca^{2+}, Zn^{2+} and Fe^{2+} (the order of binding energy: $Ca^{2+} \leq Zn^{2+} < Fe^{2+}$) [6, 63, 68-73] or in the degree of phosphate polymerisation (the order of binding energy: Ortho< Pyro< Poly-phosphate) [74]. Therefore, the most likely phosphates can be calcium phosphate or short-chain zinc phosphate. In addition, the Zn3s peak with a binding energy of 140.3 eV can be fitted, indicating zinc phosphate's presence. However, it only appears on the surface of tribofilm and under lower temperature conditions (marked in Fig. 9a and b).

Fig. 10 shows the S2p spectra at different temperatures where two peaks are marked. The one with a lower binding energy of 161.7 eV is derived from mono-sulphides, while the other peak at 162.3±0.1 eV is attributed to disulphide [63, 75, 76]. Raman analysis indicates the existence of iron disulphide in the FFO tribofilm, which is consistent with the XPS results. In the further peak fitting of each spectrum, there is a weak peak around 168.2 eV on the top surface of the tribofilm (not shown in Fig. 10). Such a peak is assigned to the sulphate group with less sulphonate [64, 77, 78], derived from over-based calcium sulphonate detergent.

As for Ca2p spectra in Fig. 11, two peaks, Ca2p3 and Ca2p1, appear that can be assigned to $CaSO_4/SO_3$, $CaCO_3$, $Ca(PO_4)_x$, and CaS. The first three can be inferred from the S2p, C1s, and P2p spectra, respectively, but there is no signal in both XPS and Raman spectra showing the existence of CaS. The detailed binding energy at each temperature will be discussed later. The Zn2p3 peak in Fig. 12 has the binding energy of 1022±0.2 eV, attributed to zinc phosphate [63, 70], and it only presents in the upper part of the tribofilm.

The XPS analysis of the elemental spectra illustrates that the chemical compositions of FFO tribofilm are similar at the four temperatures. The products in the depth direction are, starting from the surface, calcium carbonate/calcium sulphate, phosphate (mainly Ca), sulphide (FeS_2), and iron oxide/substrate. To further analyse the differences in each composition at different temperatures and its effect on the wear mechanism, the area and the binding energy of prominent peaks as a function of etching depth at different temperatures are compared, as shown in Fig. 13.

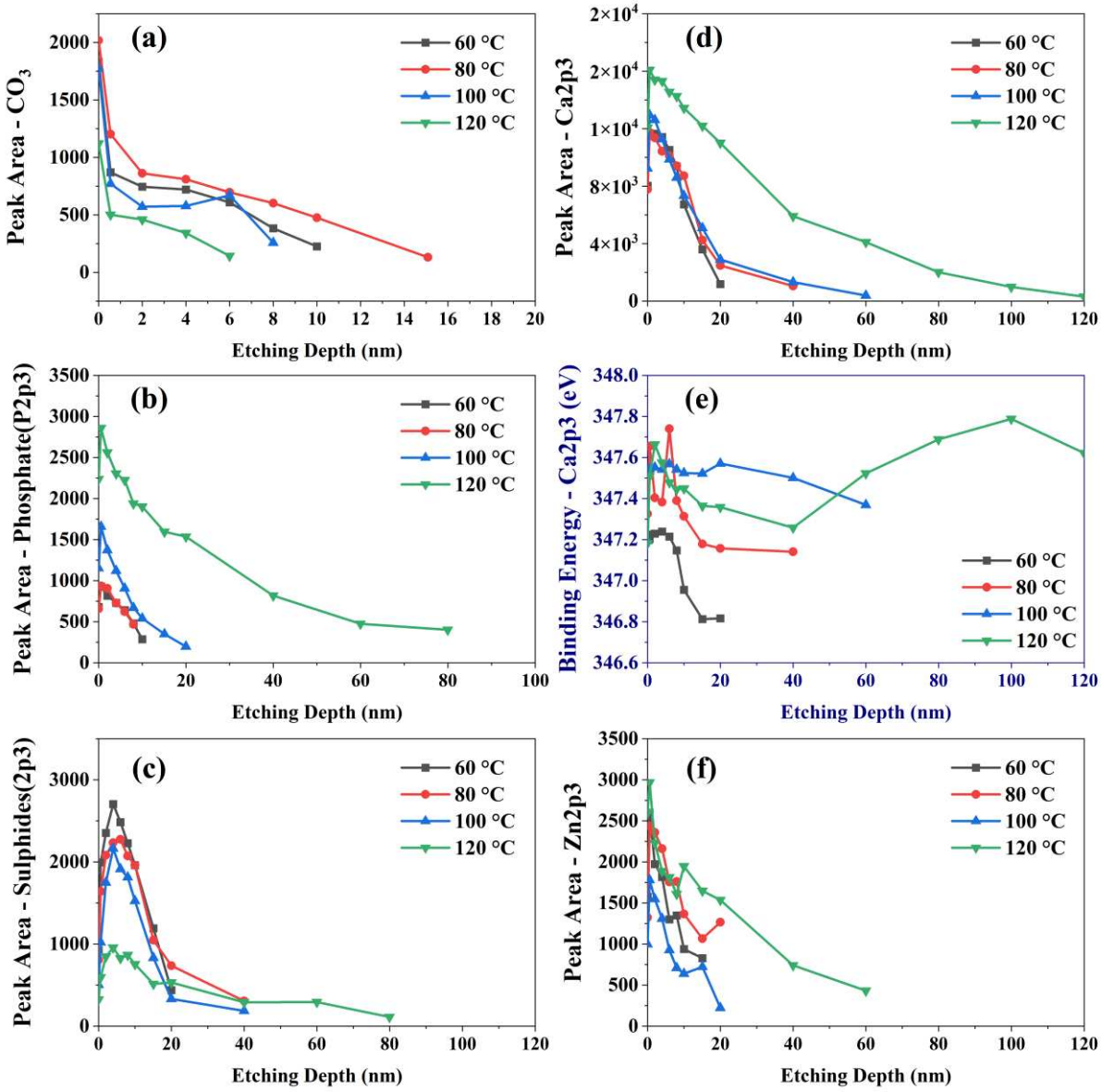

Fig. 13 The peak areas or the binding energy of the main peaks to identify the chemical compositions of the FFO tribofilm are extracted from the XPS depth profiling analysis to compare the differences at different temperatures. ((a) peak area of carbonate - C1s spectra, (b) peak area of phosphate (P 2p3) - P2p spectra, (c) peak area of sulphides (S 2p3 and S_2 2p3) - S2p spectra, (d) peak area of Ca2p3 - Ca2p spectra, (e) binding energy of Ca2p3 - Ca2p spectra and (f) peak area of Zn2p3 - Zn2p3 spectra.)

Calcium carbonate is the mineral core in the detergent. As shown in Fig. 13a, the maximum peak area of calcium carbonate appears at the top layer of the tribofilm at all temperatures but drops sharply at 0.5~2 nm from the surface. The calcium carbonate appears on the surface of the tribofilm, which is consistent with many studies on the tribofilm produced by the over-based calcium sulphonate detergent [6, 26]. By contrast, the peak area is highest at 80 °C, which seems to be similar to the wear trend. However, the author did the same tests at a lower λ ratio by changing the entrainment speed and did not find the exact correlation between calcium carbonate and wear (results are shown in Supplementary Material for brevity). Moreover, calcium carbonate may account for the antiwear property of detergents [27]. Therefore, although the influence of calcium carbonate on the wear trend cannot be excluded, it is difficult to use it alone to explain the wear mechanism.

Phosphate and sulphides should be the main compositions in the FFO tribofilm, so the peak areas of phosphate (P 2p) and sulphide (S 2p and S_2 2p) are analysed in Fig. 13b and c, respectively. At all four temperatures, the peak values of phosphate are at 0.5 nm near the surface and decrease gradually with the increase of depth (Fig. 13b). In contrast, the peak area of phosphate is almost unchanged from 60 °C to 80 °C (Phase (I) of the wear trend), whereas it increases significantly from 80°C to 120 °C (Phase (II) of the wear trend). Especially at 120 °C, the peak area and depth of phosphate have a significant increase. However, the peak area of sulphide at different temperatures shows an opposite trend to that of phosphate (see Fig. 13c), which is consistent with the Raman results. The peak area of sulphides decreases slightly from 60 °C to 100 °C. Then, there is a significant reduction from 100 °C to 120 °C. At the four temperatures, with the increased etching depth, the peak area sulphides increase rapidly from the beginning to the depth of 2 nm, reaching the maximum value, which is deeper than the peak depth of phosphate. It may indicate that part of the sulphide is covered by phosphate, which is similar to the chemical structure of the ZDDP tribofilm [14].

The Ca ion is provided only by detergents, reflecting its involvement in the tribofilm formation. At all temperature, the areas of the Ca2p3 peak decreases with the increase of depth (see Fig. 13d). At 120 °C, the peak area has the highest value. Since there are many types of calcium-containing compounds and their corresponding binding energies of Ca2p3 peaks are different, the binding energies of Ca2p3 peaks in the etching depth direction at different temperatures are further compared (see Fig. 13e). The binding energy at 60 °C is lower than those at the other temperatures, although the peak area at 60 °C is quite similar to those at 80 °C and 100 °C. This indicates that detergents participate in tribofilm formation at 60 °C to a similar extent to that at 80 °C/100 °C. However, less calcium phosphate is produced in the tribofilm at 60 °C. Therefore, it can be speculated that the antiwear properties of detergents themselves play a leading role in reducing wear at 60 °C, rather than the antiwear mechanism of the phosphates. In the range of 80~120 °C, the binding energy of the peak fluctuates between 347.4 eV and 347.7 eV at a thickness of 10 nm on the tribofilm surface, indicating the presence of calcium carbonate [64, 65, 78] and calcium sulphate [65, 77-79] on the surface. Then, the binding energy of the main part of the tribofilm is around 347.4 eV, which is attributed to calcium phosphate [68]. In addition, the binding energy increases near the substrate at 120 °C, which may also be attributed to the calcium

phosphate with higher binding energy, or from the error caused by the decrease of spectral signal when it approaches the substrate.

The other cation Zn is derived only from ZDDP. The peak areas of Zn2p3 representing zinc phosphate in the tribofilm at different temperatures are compared, as shown in Fig. 13f. It mainly exists on the surface of the tribofilm, which may be the chemisorption of ZDDP decomposition products or the intermediate product in the reaction of forming calcium phosphate. This process should occur mostly at 120 °C because the peak area of Zn2p3 has the most significant depth and the maximum value.

5 Discussions

5.1 Possible Wear Mechanisms

In this work, wear is the loss of substrate material during the rubbing, that is, the iron loss. It may mainly originate from direct contact between the two surfaces when the tribofilm is insufficient to cover the surface (mechanical wear) or be consumed in the tribochemical reactions between the surface and the additives to form the tribofilm (tribochemical wear). The wear results of FFO show that the wear rate is almost unchanged during the first 5 mins. In addition, the surface is relatively smooth, so the temperature-dependent iron loss due to mechanical wear can be ignored. Therefore, the wear mechanism of FFO mainly comes from the difference in the tribochemical wear pathway at different temperatures.

The chemical analysis of FFO tribofilm indicates that the most temperature-dependent compositions in the tribofilm are phosphates and sulphides. As the temperature increases, the signal intensity of the phosphate in tribofilm increases, while that of the iron sulphide decreases (see Fig. 6, Fig. 13b, and c). However, almost no composition can directly explain FFO's two-phase temperature-dependent wear mechanism. This indicates that the wear mechanism is not only related to the chemical composition of the reaction product (tribofilm) but also related to its formation process.

It can be seen from XPS analysis that the additives ZDDP and overbased calcium sulphonate detergent are the most involved in the formation of the FFO tribofilm. Many previous studies on the two additives have shown a competitive relationship. The primary phenomenon is that the overbased calcium sulphonate will reduce the antiwear performance of ZDDP because the Ca ion will replace the cation in zinc phosphate to form calcium phosphate [25-27]. This is also consistent with the significant phosphate detected in the FFO tribofilm. The higher amount of calcium phosphate in the FFO tribofilm at higher temperatures is the main factor in reducing wear in the Wear Phase (II).

In contrast, the wear reduction at lower temperatures in the Wear Phase (I) is thought to be dominated by the antiwear performance of the detergent itself, that is, by sulphides and calcium carbonate. The higher wear results between the two Phases are likely due to the antagonism of the two additives. This indicates that although the

wear behaviour of FFO depends on the competitive relationship between the two additives, the dominant antiwear tribofilm could change as a function of temperature, resulting in different levels of iron loss. Thus, three mechanisms are proposed to explain the wear mechanism of FFO at different temperatures, as shown in Fig. 14.

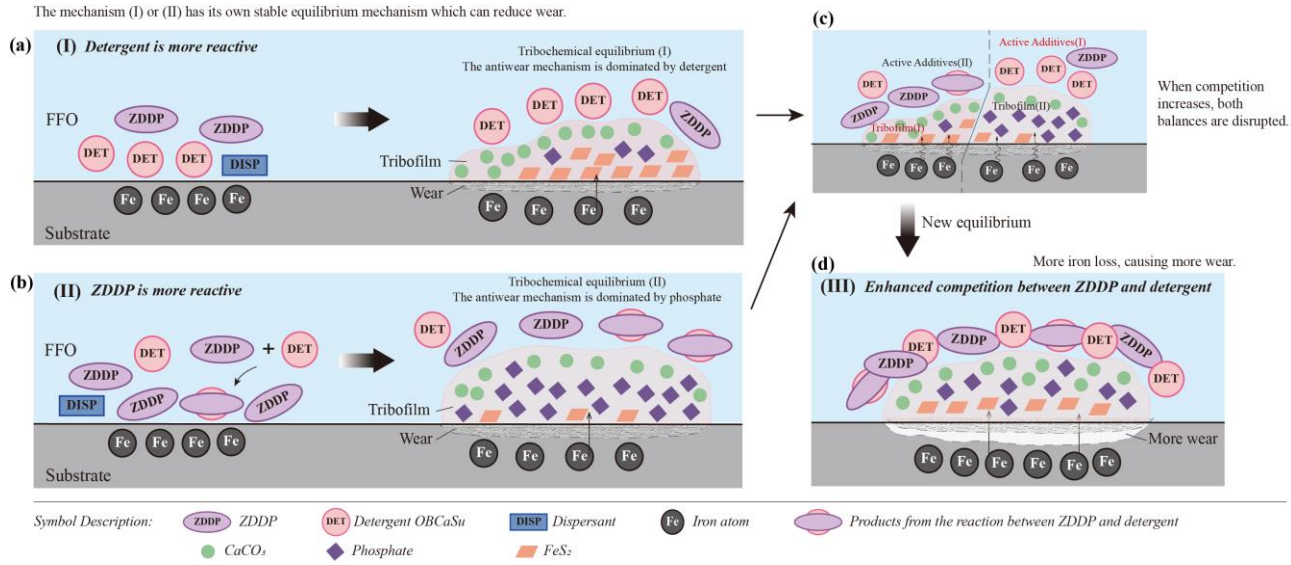

Fig. 14 Three mechanisms to explain FFO's wear mechanism at different temperatures. (a) is the Mechanism (I) when detergent is more reactive; (b) is the Mechanism (II) when ZDDP is more reactive; (c) and (d) are the Mechanism (III) when the competition is enhanced between ZDDP and detergent.

- Mechanism (I) The reactivity of detergent is greater than that of ZDDP

Suppose detergent preferentially reacts with the iron surface to form a boundary film of crystalline $CaCO_3$ or CaO. In this case, it can prevent or reduce the reaction of ZDDP with the substrate (see Fig. 14a). This can happen at low temperatures because the reaction activity of ZDDP with the substrate is weak. In this case, it seems to be less iron consumption in this tribochemical path because the generation of boundary film hardly needs the participation of iron [15]. Therefore, the iron may be lost by forming iron sulphide or by direct contact due to inadequate protection by the tribofilm. Iron sulphides have been reported to increase the lubricity of the surface [51, 52] and can reduce abrasion to a certain extent [80-82]. In addition, calcite ($CaCO_3$) film has a certain degree of resistance to wear [5, 20, 23, 28, 83]. This may be why although the tribofilm thickness is the lowest at 60 °C, the wear volume is still low.

- Mechanism (II) ZDDP is more reactive than detergent

For ZDDP, phosphate has antiwear properties under mild wear conditions [9]. The chemical analysis of FFO tribofilm shows that the peak assigned to phosphate at 120 °C has a higher signal intensity than that at 100 °C. In Phase (II) of the wear mechanism, wear decreases with increasing temperature. This also reflects the wear resistance of phosphate, although it is the calcium phosphate mainly present in FFO tribofilm rather than zinc phosphate. Kasrai *et al.* proposed two possible reaction paths for the formation of calcium phosphate by ZDDP

and calcium detergent: (1) ZDDP decomposes and then reacts with Ca^{2+}; and (2) polyphosphate produced by ZDDP, decomposes and reacts to form calcium phosphate [27]. Therefore, in the higher temperature range, when ZDDP is more reactive than the detergent, the antiwear property of phosphate plays a dominant role in reducing wear. In this way, the iron in the substrate is consumed by tribochemical reactions to supplement the tribofilm removed during the rubbing process, as shown in Fig. 14b.

- Mechanism (III) Strong competition between ZDDP and detergents

Mechanisms (I) and (II) reflect the detergent's and ZDDP's advantages in reducing wear, respectively. However, suppose that both additives are highly reactive. As shown in Fig. 14c, when the competition is enhanced, the tribofilm formed in Mechanism (I) faces the active additive environment in Mechanism (II) or the reverse, disrupting the chemical equilibrium, so the antiwear property of either of them cannot perform well. Then, the unstable tribofilm forms at the beginning and increases friction, causing higher wear. Finally, it will achieve a new equilibrium (see Fig. 14d). This may explain why there is a 'growth - reduction - regrowth' process for the growth rate of the tribofilm at 80 °C and 100 °C. Moreover, the wear and the initial friction coefficient are higher at both temperatures. Although this process is difficult to represent in terms of specific chemical reaction formula, it can be inferred that the path of iron loss is still related to the consumption in the tribochemical reaction of the tribofilm formation.

As for the mild wear mechanism when using FFO on the steel surface, the iron content in tribofilm can directly reflect the consumption of the steel substrate (iron loss) in tribochemical reaction, and it is also a way to unify the above three possible mechanisms. This provides an experimental basis for developing a wear model involving the tribochemistry of FFO.

5.2 Effect of Dispersant

Dispersants can form complexes with ZDDP molecules [8, 30-32] and affect the contact between ZDDP and metal surfaces [33-35]. Suppose the dispersant is involved in tribofilm formation, specifical succinimide in this study. In this case, the N atom should be detected in tribofilm [84], but there is no N signal from the depth profile analysis of XPS. Therefore, the influence of the dispersant on the composition of tribofilm appears to be minimal. However, the dispersant was reported to increase the decomposition temperature of ZDDP [20]. Martin *et al.* found that the dispersant can reduce the chemisorption of ZDDP and phosphate formation at 60 °C [85]. This could be why FFO tribofilm has the highest peak signal of phosphate at 120 °C and reduces wear. The corresponding antiwear mechanism when using FFO at this temperature is similar to ZDDP. This mechanism of reducing wear through phosphate appears to operate at higher temperatures in the FFO tested than in ZDDP-only lubricant.

6 Conclusions

This paper studied the wear mechanism for an FFO typically used in hydraulic piston pumps, which contains the antiwear additive ZDDP, detergents, and dispersant. Here are some findings summarised as follows.

Firstly, the growth of FFO tribofilm has a similar trend to the tribofilm formed by ZDDP alone in the base oil, including a growth phase and a stable phase. However, a two-phase temperature-dependent wear trend on the steel surfaces is exhibited when using FFO in the tested temperature range. That is, wear increases first (Phase I) and then decreases (Phase II) with the increase in tribofilm thickness/temperature.

Secondly, the wear mechanism for the FFO is related to the chemical composition and the formation process of the tribofilm. Both Raman and XPS analysis found that the most temperature-dependent compositions are phosphate and sulphide. As the temperature increases, the intensity of the phosphate peak increases, while that of the iron sulphide peak decreases.

Thirdly, a hypothesis of the mechanisms of priority reaction or enhanced competition between ZDDP and the overbased calcium sulphonate detergent is proposed to explain the wear characteristics for FFO from the perspective of iron consumption in the tribochemical reactions path. Specifically, the lower wear in Phase (I) and (II) is mainly attributed to the detergent's antiwear property and the phosphate-based antiwear mechanism provided by ZDDP, respectively. The higher wear between the two Phases is due to the increased antagonism between the two additives.

In further work, the FFO's experimental data and wear mechanism will be applied to develop the wear model in Part (II) of this series of papers.

References

1. Holmberg, K. and A. Erdemir, *Influence of tribology on global energy consumption, costs and emissions.* Friction, 2017. **5**(3): p. 263-284.

2. Holmberg, K., et al., *Global energy consumption due to friction and wear in the mining industry.* Tribology International, 2017. **115**: p. 116-139.

3. Givens, W., et al., *Hydraulic fluids.* Fuels and Lubricants Handbook, 2003.

4. Costello, M.T., *Study of Surface Films of Amorphous and Crystalline Overbased Calcium Sulfonate by XPS and AES.* Tribology Transactions, 2006. **49**(4): p. 592-597.

5. Najman, M., et al., *Combination of ashless antiwear additives with metallic detergents: interactions with neutral and overbased calcium sulfonates.* Tribology International, 2006. **39**(4): p. 342-355.

6. Costello, M.T. and R.A. Urrego, *Study of Surface Films of the ZDDP and the MoDTC with Crystalline and Amorphous Overbased Calcium Sulfonates by XPS.* Tribology Transactions, 2007. **50**(2): p. 217-226.

7. Yin, Z., et al., *Application of soft X-ray absorption spectroscopy in chemical characterization of antiwear films generated by ZDDP Part II: the effect of detergents and dispersants.* Wear, 1997. **202**(2): p. 192-201.

8. Zhang, J., E. Yamaguchi, and H. Spikes, *The antagonism between succinimide dispersants and a secondary zinc dialkyl dithiophosphate.* Tribology Transactions, 2014. **57**(1): p. 57-65.

9. Sakamoto, T., et al., *The reaction layer formed on steel by additives based on sulphur and phosphorus compounds under conditions of boundary lubrication.* Wear, 1982. **77**(2): p. 139-157.

10. Fujita, H. and H. Spikes, *The formation of zinc dithiophosphate antiwear films.* Proceedings of the Institution of Mechanical Engineers, Part J: Journal of Engineering Tribology, 2004. **218**(4): p. 265-278.

11. Taylor, L., A. Dratva, and H.A. Spikes, *Friction and Wear Behavior of Zinc Dialkyldithiophosphate Additive.* Tribology Transactions, 2000. **43**(3): p. 469-479.

12. Fujita, H., R. Glovnea, and H. Spikes, *Study of zinc dialkydithiophosphate antiwear film formation and removal processes, part I: experimental.* Tribology transactions, 2005. **48**(4): p. 558-566.

13. Fuller, M.S., et al., *The use of X□ray absorption spectroscopy for monitoring the thickness of antiwear films from ZDDP.* Tribology Letters, 2000. **8**(4): p. 187-192.

14. Spikes, H., *The history and mechanisms of ZDDP.* Tribology letters, 2004. **17**(3): p. 469-489.

15. Mansot, J., M. Hallouis, and J. Martin, *Colloidal antiwear additives 2. Tribological behaviour of colloidal additives in mild wear regime.* Colloids and Surfaces A: Physicochemical and Engineering Aspects, 1993. **75**: p. 25-31.

16. Giasson, S., et al., *Study of boundary film formation with overbased calcium sulfonate by PM-IRRAS spectroscopy.* Thin Solid Films, 1994. **252**(2): p. 111-119.

17. Cizaire, L., et al., *Tribochemistry of overbased calcium detergents studied by ToF-SIMS and other surface analyses.* Tribology Letters, 2004. **17**(4): p. 715-721.

18. Costello, M.T., R.A. Urrego, and M. Kasrai, *Study of surface films of crystalline and amorphous overbased sulfonates and sulfurized olefins by X-ray absorption near edge structure (XANES) spectroscopy.* Tribology Letters, 2007. **26**(2): p. 173-180.

19. Topolovec-Miklozic, K., T.R. Forbus, and H. Spikes, *Film Forming and Friction Properties of Overbased Calcium Sulphonate Detergents.* Tribology Letters, 2008. **29**(1): p. 33-44.

20. Shirahama, S. and M. Hirata, *The effects of engine oil additives on valve train wear.* Lubrication Science, 1989. **1**(4): p. 365-384.

21. Delfort, B., M. Born, and B. Daoudal, *Functionalization of overbased calcium sulfonates-synthesis and evaluation of antiwear and extreme-pressure performances.* Lubrication Engineering, 1995: p. Medium: X; Size: pp. 981-990.

22. Delfort, B., B. Daoudal, and L. Barré, *Particle size determination of (functionalized) colloidal calcium carbonate by small angle x-ray scattering—Relation with antiwear properties.* Tribology transactions, 1999. **42**(2): p. 296-302.

23. Minami, I., et al., *Tribochemical approach toward mechanism for synergism of lubricant additives on antiwear and friction reducing properties*, in *Tribology and Interface Engineering Series*, D. Dowson, et al., Editors. 2005, Elsevier. p. 259-268.

24. Willermet, P., et al., *Formation, structure, and properties of lubricant□derived antiwear films.* Lubrication Science, 1997. **9**(4): p. 325-348.

25. Kasrai, M., et al., *Study of the effects of Ca sulfonate on antiwear film formation by X-ray absorption spectroscopy using synchrotron radiation.* Journal of synchrotron radiation, 1999. **6**(3): p. 719-721.

26. Wan, Y., et al., *Effects of detergent on the chemistry of tribofilms from ZDDP: studied by X-ray absorption spectroscopy and XPS*, in *Tribology series*. 2002, Elsevier. p. 155-166.

27. Kasrai, M., et al., *X-Ray Absorption Study of the Effect of Calcium Sulfonate on Antiwear Film Formation Generated From Neutral and Basic ZDDPs: Part 1—Phosphorus Species.* Tribology Transactions, 2003. **46**(4): p. 534-542.

28. Kasrai, M., et al., *X-Ray Absorption Study of the Effect of Calcium Sulfonate on Antiwear Film Formation Generated From Neutral and Basic ZDDPs: Part 2 — Sulfur Species.* Tribology Transactions, 2003. **46**(4): p. 543-549.

29. Booth, J.E., *The feasibility of using electrostatic charge condition monitoring for lubricant additive screening*, *University of Southampton*. 2008.

30. Gallopoulos, N.E. and C.K. Murphy, *Interactions between a zinc dialkylphosphorodithioate and lubricating oil dispersants.* ASLE TRANSACTIONS, 1971. **14**(1): p. 1-7.

31. Inoue, K. and H. Watanabe, *Interactions of engine oil additives.* ASLE transactions, 1983. **26**(2): p. 189-199.

32. Shiomi, M., et al., *Interaction between zinc dialkyldithiophosphate and amine.* Lubrication Science, 1989. **1**(2): p. 131-147.

33. Rounds, F., *Changes in friction and wear performance caused by interactions among lubricant additives.* Lubrication Science, 1989. **1**(4): p. 333-363.

34. Zhang, Z., et al., *Study of the Interaction of ZDDP and Dispersants Using X-ray Absorption Near Edge Structure Spectroscopy—Part 1: Thermal Chemical Reactions.* Tribology Letters, 2003. **15**(4): p. 377-384.

35. Plaza, S., *The Effect of Other Lubricating Oil Additives on the Adsorption of Zinc Di-Isobutyldithiophosphate on Fe and γ-Fe2O3 Powders.* ASLE transactions, 1987. **30**(2): p. 241-247.

36. Kosarieh, S., et al., *Tribological performance and tribochemical processes in a DLC/steel system when lubricated in a fully formulated oil and base oil.* Surface and Coatings Technology, 2013. **217**: p. 1-12.

37. Aota, H., et al., *Tribological Properties of Nitrided Steels Lubricated with Fully Formulated Oils in Boundary Lubrication Condition.* Tribology Online, 2018. **13**(3): p. 166-171.

38. Pereira, G., et al., *Chemical and mechanical analysis of tribofilms from fully formulated oils Part 1 – Films on 52100 steel.* Tribology - Materials, Surfaces & Interfaces, 2013. **1**(1): p. 48-61.

39. Wan, S., et al., *Tribochemistry of adaptive integrated interfaces at boundary lubricated contacts.* Sci Rep, 2017. **7**(1): p. 9935.

40. Taylor, L.J. and H. Spikes, *Friction-enhancing properties of ZDDP antiwear additive: part I—friction and morphology of ZDDP reaction films.* Tribology transactions, 2003. **46**(3): p. 303-309.

41. Topolovec-Miklozic, K., T.R. Forbus, and H.A. Spikes, *Film thickness and roughness of ZDDP antiwear films.* Tribology Letters, 2007. **26**(2): p. 161-171.

42. Shimizu, Y. and H.A. Spikes, *The influence of slide–roll ratio on ZDDP tribofilm formation.* Tribology Letters, 2016. **64**(2): p. 19.

43. Ghanbarzadeh, A., et al., *A semi-deterministic wear model considering the effect of zinc dialkyl dithiophosphate tribofilm.* Tribology Letters, 2016. **61**(1): p. 12.

44. Ghanbarzadeh, A., et al., *Development of a new mechano-chemical model in boundary lubrication.* Tribology International, 2016. **93**: p. 573-582.

45. Ueda, M., A. Kadiric, and H. Spikes, *On the Crystallinity and Durability of ZDDP Tribofilm.* Tribology Letters, 2019. **67**(4).

46. Ueda, M., H. Spikes, and A. Kadiric, *In-situ observations of the effect of the ZDDP tribofilm growth on micropitting.* Tribology International, 2019. **138**: p. 342-352.

47. ISO, *6743-4:2015 Lubricants, industrial oils and related products (class L) — Classification — Part 4: Family H (Hydraulic systems)*. 2015, British Standars Insititution.

48. Totten, G.E. and V.J. De Negri, *Handbook of hydraulic fluid technology, second edition*. 2ed ed. CRC Press. 2011.

49. Benedet, J., et al., *Spurious mild wear measurement using white light interference microscopy in the presence of antiwear films.* Tribology Transactions, 2009. **52**(6): p. 841-846.

50. Tripaldi, G., A. Vettor, and H. Spikes, *Friction behaviour of ZDDP films in the mixed, boundary/EHD regime.* SAE transactions, 1996: p. 1819-1830.

51. Peng, T., et al., *Solid FeS lubricant: a possible alternative to MoS2 for Cu–Fe-based friction materials.* International Journal of Minerals, Metallurgy, and Materials, 2017. **24**(11): p. 1278-1283.

52. Peng, T., et al., *Low-cost solid FeS lubricant as a possible alternative to MoS2 for producing Fe-based friction materials.* International Journal of Minerals, Metallurgy, and Materials, 2017. **24**(1): p. 115-121.

53. Song, C., et al., *Hydrothermal synthesis of iron pyrite (FeS2) as efficient counter electrodes for dye-sensitized solar cells*. Solar Energy, 2016. **133**: p. 429-436.

54. Lafuente, B., et al., *1. The power of databases: The RRUFF project*, in *Highlights in mineralogical crystallography*. 2015, De Gruyter (O). p. 1-30.

55. Liu, T., et al., *Enhanced Raman intensity in ZnS planar and channel waveguide structures via carbon ion implantation.* Optical Materials, 2021. **112**: p. 110733.

56. Kim, J.H., et al., *Raman spectroscopy of ZnS nanostructures.* Journal of Raman Spectroscopy, 2012.

57. Avril, C., et al., *Raman spectroscopic properties and Raman identification of CaS-MgS-MnS-FeS-Cr2FeS4 sulfides in meteorites and reduced sulfur-rich systems.* Meteoritics & Planetary Science, 2013. **48**(8): p. 1415-1426.

58. Gachot, C., et al., *Microstructural and Chemical Characterization of the Tribolayer Formation in Highly Loaded Cylindrical Roller Thrust Bearings.* Lubricants, 2016. **4**(2): p. 19.

59. Faruck, A.A.M., et al., *How lubricant formulations and properties influence the performance of rotorcraft transmissions under loss of lubrication conditions.* Tribology International, 2020. **151**: p. 106390.

60. Brow, R.K., et al., *The short-range structure of zinc polyphosphate glass.* Journal of Non-Crystalline Solids, 1995. **191**(1-2): p. 45-55.

61. Kazanci, M., et al., *Complementary information on in vitro conversion of amorphous (precursor) calcium phosphate to hydroxyapatite from Raman microspectroscopy and wide-angle X-ray scattering.* Calcified tissue international, 2006. **79**(5): p. 354-359.

62. Berkani, S., et al., *Structural Changes in Tribo-Stressed Zinc Polyphosphates.* Tribology Letters, 2013. **51**(3): p. 489-498.

63. Heubergera, R. and A.R.a.N.D.S. , *XPS study of the influence of temperature on ZnDTP tribofilm composition.* 2007.

64. Cizaire, L., et al., *Chemical analysis of overbased calcium sulfonate detergents by coupling XPS, ToF-SIMS, XANES, and EFTEM.* Colloids and Surfaces A: Physicochemical and Engineering Aspects, 2004. **238**(1-3): p. 151-158.

65. Biesinger, M., *X-ray Photoelectron Spectroscopy (XPS) reference pages.* Surface Science Western, University of Western Ontario, Ontario, 2015.

66. Li, Y., et al., *Atomically Defined Iron Carbide Surface for Fischer–Tropsch Synthesis Catalysis.* ACS Catalysis, 2019. **9**(2): p. 1264-1273.

67. Furlan, A., et al., *Structure and bonding in amorphous iron carbide thin films.* Journal of Physics: Condensed Matter, 2015. **27**(4): p. 045002.

68. Chusuei, C.C., et al., *Calcium phosphate phase identification using XPS and time-of-flight cluster SIMS.* Analytical chemistry, 1999. **71**(1): p. 149-153.

69. Crobu, M., et al., *Tribochemistry of bulk zinc metaphosphate glasses.* Tribology letters, 2010. **39**(2): p. 121-134.

70. Minfray, C., et al., *A multi-technique approach of tribofilm characterisation.* Thin Solid Films, 2004. **447**: p. 272-277.

71. Wang, Y. and P.M. Sherwood, *Iron (III) phosphate (FePO4) by XPS.* Surface Science Spectra, 2002. **9**(1): p. 99-105.

72. Wang, Y., D.J. Asunskis, and P.M.A. Sherwood, *Iron (II) Phosphate (Fe3(PO4)2 by XPS.* Surface Science Spectra, 2002. **9**(1): p. 91-98.

73. Liu, Y., et al., *Synthesis of different structured FePO4 for the enhanced conversion of methyl cellulose to 5-hydroxymethylfurfural.* RSC Advances, 2017. **7**(81): p. 51281-51289.

74. Crobu, M., et al., *Chain-length-identification strategy in zinc polyphosphate glasses by means of XPS and ToF-SIMS.* Analytical and bioanalytical chemistry, 2012. **403**(5): p. 1415-1432.

75. Chaturvedi, S., et al., *XPS and LEED study of a single-crystal surface of pyrite.* American Mineralogist, 1996. **81**(1-2): p. 261-264.

76. Mattila, S., J. Leiro, and K. Laajalehto, *Surface XPS core-level shifts of FeS2.* Applied surface science, 2003. **212**: p. 97-100.

77. Bahadur, S., D. Gong, and J. Anderegg, *Investigation of the influence of CaS, CaO and CaF2 fillers on the transfer and wear of nylon by microscopy and XPS analysis.* Wear, 1996. **197**(1-2): p. 271-279.

78. Luque, A., et al., *Analysis of the surface of different marbles by X-ray photoelectron spectroscopy (XPS) to evaluate decay by SO 2 attack.* Environmental earth sciences, 2013. **68**(3): p. 833-845.

79. Nyenge, R.L., H.C. Swart, and O.M. Ntwaeaborwa, *Luminescent properties, intensity degradation and X-ray photoelectron spectroscopy analysis of CaS:Eu2+ powder.* Optical Materials, 2015. **40**: p. 68-75.

80. Wang, H.-D., et al., *Characterization and tribological properties of plasma sprayed FeS solid lubrication coatings.* Materials characterization, 2005. **55**(1): p. 43-49.

81. Wang, H.-d., et al., *Investigation on friction and wear behaviors of FeS films on L6 steel surface.* Applied Surface Science, 2005. **252**(4): p. 1084-1091.

82. Lee, I. and I. Park, *Solid lubrication coating of FeS layer on the surface of SKD 61 steel produced by plasma sulfnitriding.* Surface and Coatings Technology, 2006. **200**(11): p. 3540-3543.

83. Morizur, M. and O. Teysset, *Antiwear actions of additives in solid dispersion.* Lubrication Science, 1992. **4**(4): p. 277-299.

84. Yamaguchi, E.S., et al., *Study of the Interaction of ZDDP and Dispersants Using X-ray Absorption Near Edge Structure Spectroscopy—Part 2: Tribochemical Reactions.* Tribology Letters, 2003. **15**(4): p. 385-394.

85. Martin, J., et al., *Role of nitrogen in tribochemical interaction between Zndtp and succinimide in boundary lubrication.* Tribology International, 2000. **33**(7): p. 453-459.

Experimental and Numerical Study on Wear Characteristics of Steel Surfaces Involving the Tribochemistry of a Fully Formulated Oil Part I: Experiments

Yajing Gong[a*], Ardian Morina[a*], Chun Wang[a], Yuechang Wang[a], Yukio Tamura[b], Akihito Ishihara[b], Ali Ghanbarzadeh[a], Anne Neville[a]

* Corresponding authors: artemisgong@hotmail.com (Yajing Gong); a.morina@leeds.ac.uk (Ardian Morina)
a Institute of Functional Surfaces, School of Mechanical Engineering, University of Leeds, Leeds, LS2 9JT, United Kingdom
b Manufacturing Engineering Development Centre, Production Division, Komatsu Ltd., Osaka 573-1011, Japan

Abstract:

This paper studied a fully formulated oil (FFO) in the hydraulic piston pump, containing mainly zinc dialkyldithiophosphate (ZDDP), detergents, and dispersants. The results of tribo-tests show that the antiwear characteristics are different when using FFO compared to using a single additive oil such as base oil + ZDDP. A two-phase temperature-dependent wear trend was found when FFO is used. Phase (I) is in the low-temperature range, where wear increases with increasing tribofilm thickness and temperature. Phase (II) is in the high-temperature range where the tribofilm thickness increases but wear decreases as the temperature increases. Raman spectroscopy and X-ray photoelectron spectroscopy (XPS) analysis of the tribofilm show that the most temperature-dependent compositions are phosphate and iron sulphides, where the signal intensity of phosphates increases, but that of sulphides decreases when the temperature increases. It indicates that the participation of detergent and ZDDP in the tribofilm formation increases at low and high temperatures, respectively. However, no signal shows the dispersant participating in the tribofilm formation. A hypothesis of mechanisms of reaction priority or enhanced competition among different additives at different temperatures is proposed from the iron loss perspective to explain the two-phase temperature-dependent wear mechanism. This study also provides the experimental basis for the wear modelling involving the tribochemistry of FFO in Part (II) of the research series.

Keywords: Fully Formulated Oil; Wear; ZDDP; Detergent

1 Introduction

Wear is an important reason for affecting machinery life and increasing maintenance costs in the industry [1, 2]. Mild wear can lead to reduced machine efficiency, while severe wear can lead directly to the failure of the machine. Lubrication is one of the commonly used methods to reduce wear. However, it is difficult to prevent the wear between relatively moving components/parts, such as piston/cylinder or gear pairs, due to lubricant

starvation caused by mechanical vibration or fit errors. In the hydraulic system, hydraulic fluids perform the functions of lubrication and heat dissipation like conventional lubricants and energy transmission [3]. This requires the hydraulic lubricants to have antiwear behaviour and stable performances in other aspects, such as cleaning the contaminants and preventing oxidation.

Fully formulated oils (FFO) contain various additives (such as antiwear additives, detergents, dispersants, and antioxidants), which are added to the base oil (such as mineral oil and synthetic oil) with a specific concentration. They are used to fulfil the multifunctionality in applications. However, since FFOs have high levels of chemical complexity, it is challenging to study the effect of detailed compositions of FFO on antiwear performance and wear prediction. Decades of research on each kind of additive or its combinations have shown that additives' type, concentration, acidity, and alkalinity affect their antiwear behaviours. The same additive may perform differently under different working conditions [4-9].

Zinc dialkyldithiophosphate (ZDDP) is a widely used antiwear additive. Film formation is a significant function of ZDDP. Many studies showed that tribofilm only formed within the rubbing tracks [10, 11] and that the tribofilm thickness stabilises over 50~150 nm on steel surfaces [10, 12, 13]. The formation rate of tribofilm increases with the increase in temperature and concentration of ZDDP [12]. The main compositions from the tribofilm surface to the substrate are alkylphosphate precipitates, polyphosphate (Zn), phosphate (Zn/Fe), and Fe/Zn sulphides near the substrate [14]. It was found that the antiwear effect of ZDDP is mainly derived from the formation of phosphates [9].

The primary function of detergents is to clean the acidic substances in the lubricant, so it is usually alkaline or neutral. Over-based calcium sulphonate is a commonly used detergent that can form a boundary film on the steel surface that contains mainly calcium carbonate and/or CaO [4, 6, 15-18]. It has been found that the tribofilm formed by the overbased calcium sulphonate detergent can grow to 160 nm in 2 hours [19], but its formation process is different from ZDDP, which does not require much iron to be involved [15]. Although the overbased calcium sulphonate detergent was found to have antiwear and anti-scuffing properties [5, 15, 20-23], it was reported when combined with ZDDP to have an antagonistic effect on the antiwear performance of ZDDP [24-28].

The primary role of dispersants is to keep insoluble substances suspended in oil and avoid deposition on the surface. It usually contains a higher molecular weight that can help maintain the oil viscosity. Most dispersants are considered to have little effect on wear or friction [29]. However, some studies have shown that dispersants and ZDDP have antagonistic effects on wear reduction due to complexation [8, 30-32]. In addition, the dispersant may adsorb or react with metal surfaces [33-35] or dissolve the existing ZDDP tribofilm [8], which will also reduce the effectiveness of the antiwear properties of ZDDP.

The antiwear performances of single additive or combinations of different additives have been well studied for many years. However, it still cannot answer the performance of the FFO as a whole, even if the type, concentration, and other information of additives contained in the FFO are known. In recent years, more experimental studies have used FFOs to study antiwear performance [36-39]. One aspect of FFO studies is to evaluate the performance of the additives contained therein on different material surfaces. On the other hand, the interaction between multiple additives can be more abundantly and directly understood by comparing their combined behaviour with that of a single additive. Experimental testing is the primary method for studying the antiwear performance of FFOs. However, experimentally understanding the wear mechanism is not enough for FFO users to monitor the machine's service life. Advanced modelling and numerical simulation techniques are also necessary to quantify the wear process and predict failures.

Therefore, this work studied a commercial FFO used in the hydraulic system, containing the antiwear additive ZDDP, detergents overbased calcium sulphonate and phenate, and the dispersant succinimide. A two-part series of papers are organised to report the experimental findings, and theoretical modelling works. This paper, the first part, presents an experimental study on the wear mechanism involving the FFO and its tribochemistry under different temperatures. The experimental results are then used for the modelling work to establish the theory and to simulate the main tribological phenomena such as tribofilm growth and wear evolution, which will be discussed in Part (II) of the research series.

2 Methodology

2.1 MTM-SLIM

Tribotests are conducted by Mini Traction Machine with the Spacer Layer Imaging Method (MTM-SLIM, PCS Instruments, UK), as shown in Fig. 1. The MTM is a tribometer with a ball-on-disc configuration (see Fig. 1a), which allows the rotation speed of the ball and disc to be adjusted independently to achieve different sliding/rolling conditions. The SLIM is an external component of the MTM for testing the *in-situ* growth process of the tribofilm and analysing the thickness after the test, which has been widely used in many studies of ZDDP tribofilm [10, 12, 40-46]. The main principle is shown in Fig. 1b. Through a lens (consisting of a glass flat, a thin semi-reflective chromium layer and a silica spacer layer), a white light source and its reflected light from the steel surface produce an interference image of the tribofilm, which is captured by a colour camera and microcomputer. After the test, the RGB colour of each pixel in the image is analysed by offline software, and the tribofilm thickness is calculated automatically.

The ball has a diameter of 3/4 inch (~19 mm) with a roughness of 20 nm (Ra), and the disc has a diameter of 46 mm with a roughness of 10 nm. The material of both the ball and the disc is AISI52100 steel. The lubricant is a hydraulic FFO (provided by Komatsu Ltd., Japan), and its specifications are listed in Table 1. The base oil in the FFO is a low viscosity mineral oil with a kinetic viscosity of 36 cSt at 40 °C and 5.9 cSt at 100 °C. The main

additives are a mixture of primary and secondary ZDDPs, overbased calcium sulphonate, overbased calcium phenate, and succinimide.

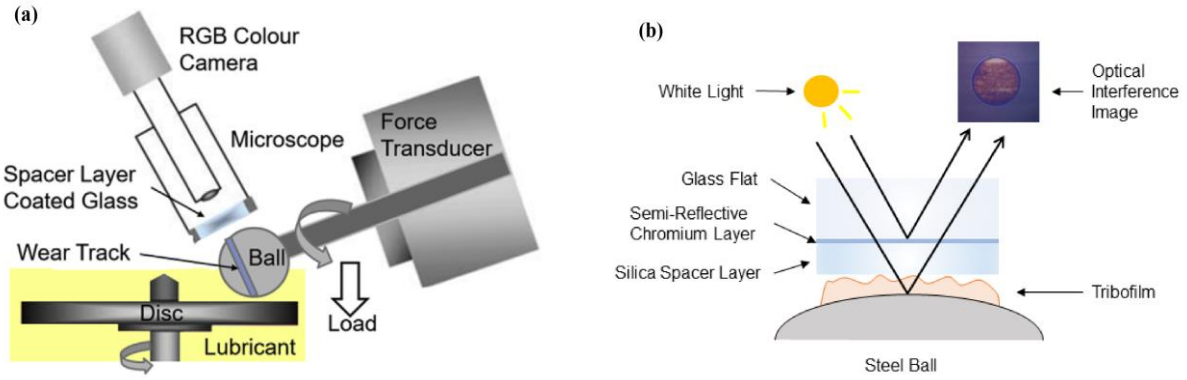

Fig. 1 a) Schematic diagram of MTM-SLIM [46]; b) SLIM principle.

Table 1 Specification of the FFO.

Fully Formulated Oil	**Types**
Base Oil	Mineral Oil (Kinetic viscosity: 36 cSt at 40 °C, 5.9 cSt at 100 °C)
Antiwear Additive	Primary and Secondary ZDDP (0.08 wt.% P)
Detergents	Over-based calcium sulphonate/phenate (0.38 wt.% Ca)
Dispersant	Succinimide

Considering the application of hydraulic piston pumps, the test conditions are designed in Table 2. According to the ISO 6743-4 hydraulic fluid classification system [47], the operating temperature range of mineral oils with antiwear additives is about -10 °C ~ 90 °C. However, for some high-temperature applications, the upper-temperature limit can reach 120 °C [48], so the main test temperatures in this study are 60, 80, 100, and 120 °C. The load is 60 N to have an equivalent maximum Hertzian pressure of 1.2 GPa. The entrainment speed is 100 mm/s, and the slide-to-roll ratio (SRR) is 150 %. The tests are designed in a boundary lubrication regime. The maximum test duration is 6 hours, and there are different test intervals for wear measurements.

Table 2 Working conditions for MTM-SLIM tests

Traction Mode	
Temperatures	60, 80 100 and 120 °C
Load	60 N
Entrainment Speed	100 mm/s
SRR	150 %
Duration	6h with different intervals

Before testing, heptane is first used to clean the antirust oil and dust on the surface of the samples with soft tissue. Then, the samples are immersed in an acetone solution and cleaned in an ultrasonic bath for 30 mins. Finally, the samples are rinsed with methanol and dried naturally. After the MTM tests, the samples are rinsed with heptane to remove the remained lubricants on the surface and then dried naturally.

2.2 White Light Interferometry

The wear measurements were carried out by white light interferometry (NPFLEX^{TM}, Bruker, UK/USA). Since the tribofilm generated by ZDDP contains phosphate, which has light transmittance and interferes with white light interference measurement [49], the tribofilm must be removed before wear measurement. The 0.05 mol/L ethylenediaminetetraacetic (EDTA) solution was used in many studies to remove tribofilm formed by ZDDP [41, 49] and over-based calcium sulphonate detergent [19]. Thus, it is considered to apply to the tribofilm formed by FFO containing these two film-forming additives.

Wear measurement was carried out with a total magnification of 10× with a measurement area of 400×600 μm^2. The results are processed by the built-in Vision64® software, which allows the wear volume in the measured area to be calculated directly. Since tests were run at a high SRR of 150 %, the disc sliding distance is six times higher than the ball for the same test duration. The length of the disc wear track is approximately three times that of the ball, so the disc wears more than the ball. Fig. 2 shows the examples of wear results on the ball and on the disc, also indicating that the wear on the ball (Fig. 2a) is very small and hard to measure at the maximum test time, so only the wear results on the discs are discussed in the following sections.

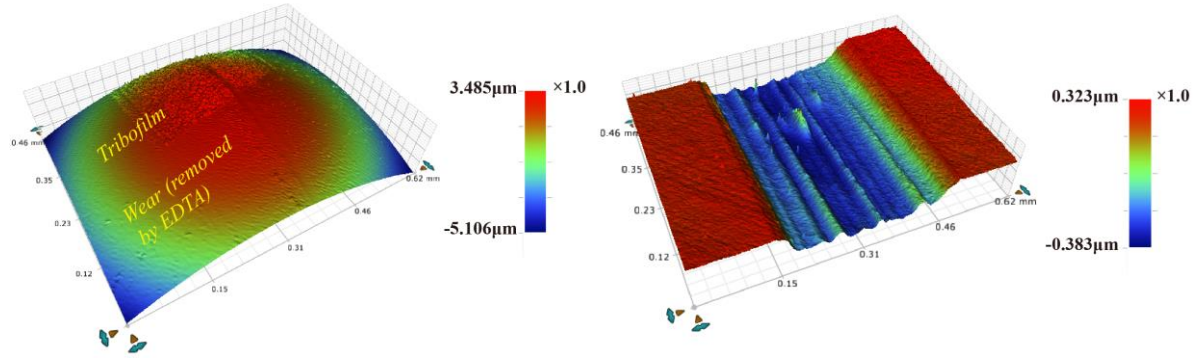

Fig. 2 The 3D images of worn surfaces on (a) the steel ball and (b) the steel disc after 6-hour testing at 100 °C, captured by NPFLEX with the magnification of 10X.

2.3 Raman Spectroscopy

Raman spectroscopy (Renishaw inVia, UK) measures mainly sulphides and phosphates in the tribofilm. The laser with the wavelength of 488 nm is chosen, and its maximum energy is 10 mW. The laser intensity is 50 %. The acquisition range is 150 cm^{-1}~1600 cm^{-1}, and the acquisition time is 30 seconds. There are 1~2 areas of the tribofilm selected randomly on the ball and disc, and 22 spectra are analysed for one test condition. The one with the strongest signal is chosen for comparison.

After obtaining the Raman spectrum, the baseline of the raw data is removed first. Then, a mixed Gaussian/Lorentzian method is used to fit the peaks to obtain the information of frequency, intensity and full width at half maximum (FWHM).

2.4 X-ray Photoelectron Spectroscopy (XPS)

The XPS instrument used in this work is the PHI5000 Versa Probe II^{TM} (ULVAC-PHI Inc., Japan/USA). Conventional XPS analysis can provide the chemical structure at the top surface of 5~10 nm [26]. However, in analogy with the tribofilm formed by ZDDP, the chemical compositions in the tribofilm should be different along with depth, so the depth profiling with the high-resolution XPS spectral analysis is used to analyse the key elements and compounds in the tribofilm from the top surface to the substrate. An Al Kα monochromatic source is used at 15 kV and 50 W with a step energy of 1486.6 eV. The test area is in the centre of the tribofilm and is approximately 200 µm in diameter. The Ar ion sputtering is applied for etching the specimens with 4 kV and 20 mA energy. The high-resolution C1s, N1s, O1s, P2p, S2p, Ca2p, Fe2p, and Zn2p3 spectra are collected at a pass energy of 23.5eV with an acquisition step size of 0.1eV. The etching rate is 18.175nm/mins as the reference of SiO_2. The maximum etching depth is about 120 nm.

The post-processing process of XPS data is performed using CasaXPS software. The Shirley-Sherwood iterative method is used for background subtraction, and Gaussian and Lorentzian functions are applied for curve-fitting

the peaks. For 2p spectra of elements P, S, and Ca, due to the splitting of the spin orbits, a doublet with an area ratio of 2:1 is set in the peak fitting.

3 Tribological Results

3.1 Tribofilm Formation

The evolution of the FFO tribofilm thickness at different temperatures is shown in Fig. 3. The growth curves of FFO tribofilm (Fig. 3a) can be divided into two phases: (I) growth phase and (II) stable phase. In the growth phase, the tribofilm thickness increases rapidly at the beginning. The growth rate primarily increases with an increase in temperature. In the stable phase, the tribofilm thickness reaches a dynamic balance that is primarily unchanged at each temperature. When the temperature rises, the average balanced thickness increases, which can grow to about 120 nm at 120 °C. The growth process of FFO tribofilm is similar to that of tribofilm formed by ZDDP with a higher carbon length [12, 41]. However, it can also be noted that the growth rate of the FFO tribofilm decreased and then increased between 15 mins and 60 mins of the test time, especially at 80 °C and 100 °C. The interferometry images of the tribofilm captured by SLIM exhibit the morphology of the tribofilm at different test durations, as shown in Fig. 3b. The tribofilm distribution appears to be more uneven in the contact at lower temperatures.

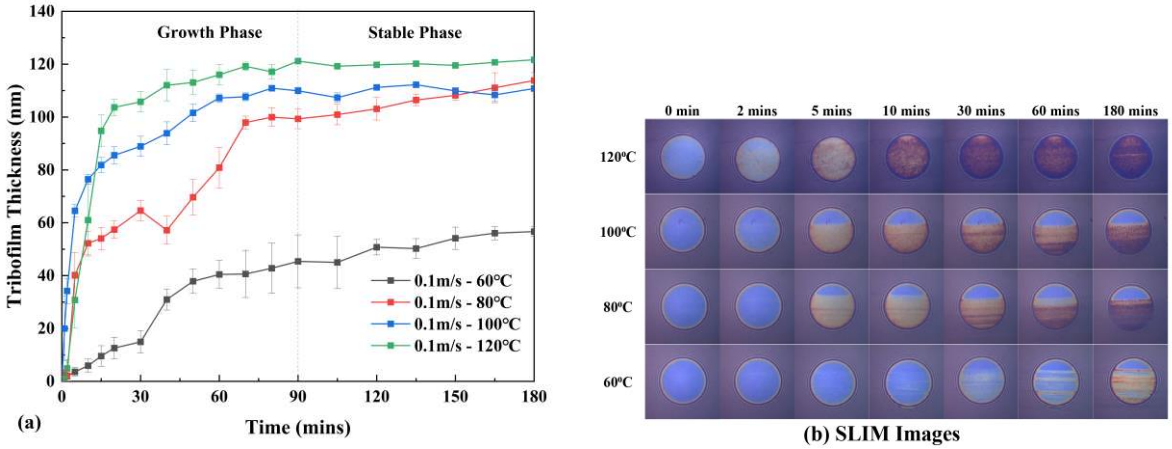

Fig. 3 MTM-SLIM results of (a) FFO tribofilm growth and (b) SLIM images at different temperatures (60, 80, 100 and 120 °C).

3.2 Friction Coefficient

Fig. 4 shows the friction coefficients corresponding to the FFO tribofilm growth process at different temperatures. As shown in Fig. 4a, all the friction coefficients in the steady-state phase increase compared to the initial values at the four tested temperatures. However, the evolution process is varied from temperature to temperature. At 60 °C, the friction coefficient experiences a slow increase and then reaches a steady state. Its growth rate and the value in the steady-state phase are the lowest of all the temperatures tested. The changes in friction coefficient are relatively similar at 80 °C and 100 °C, but the friction coefficient at 100 °C is overall

slightly higher than that at 80 °C. During the first 15 mins of the test, it increases rapidly. After a 'reduction and regrowth' process, a plateau is reached. Comparing the growth curve of the tribofilm at the same temperature in Fig. 3a, the growth rate of the tribofilm has a similar variation. The friction coefficient at 120 °C also increases rapidly before reaching a stable value, where the increase rate is lower than that at 80 °C and 100 °C. However, the friction coefficient at 120 °C in the steady-state phase has the maximum value.

The average steady-state friction coefficient and corresponding average tribofilm thickness after 90 mins of testing at each temperature are calculated, as illustrated in Fig. 4b. With the increase in temperature, the friction coefficient and the tribofilm thickness in the steady-state phase increase with a similar trend.

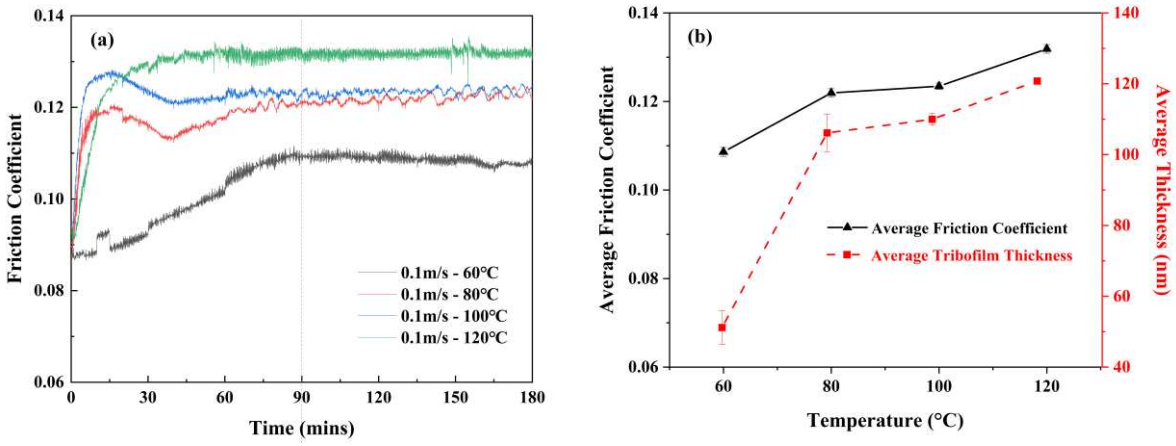

Fig. 4 MTM-SLIM results of (a) friction coefficients at different temperatures (60, 80, 100 and 120 °C) and (b) average friction coefficient at the stable phase compared with average thickness at each temperature.

Some researchers have shown that different compositions in the tribofilm may lead to differences in the friction coefficients. For example, the formation of ZDDP tribofilm can increase the friction coefficient on the steel surface [11, 50], while the formation of iron sulphide may reduce the friction coefficient [51, 52]. Therefore, the changes in friction coefficients indicate that the growth process and chemical composition of tribofilms formed at different temperatures may differ.

3.3 Wear Results

Fig. 5 shows the wear results at different temperatures. Unlike the *in-situ* tests of tribofilm thickness, the wear results are only measured after the tribotests are finished, so the increase in wear may be discontinuous at the same temperature. The wear evolution can be seen in Fig. 5a, where the highest wear occurs at 80 °C, but the results at 100 °C are very close. When the temperature increases to 120 °C, the expected wear reduction is identified due to the antiwear performance of the additives. Unexpectedly, the lowest wear occurs at 60 °C. As temperature increases from 60 °C to 80 °C, wear and tribofilm thickness increase, which does not seem to reflect

the protective effect of the tribofilm on the surface. Thus, the reasons for the wear trend in this lower temperature range must be further explored.

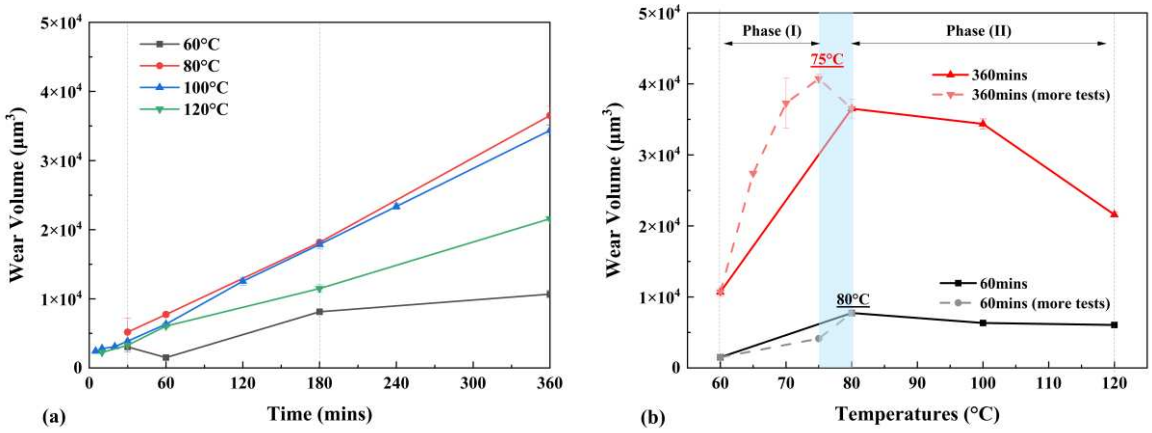

Fig. 5 Wear measurements on steel discs by NPFLEX at different temperatures: (a) evolution of wear volume; (b) wear volume as the function of the temperature at the test durations of 60 mins and 360 mins.

In order to analyse the correlation between wear and temperature more clearly, the wear data in the test duration of 60 mins and 360 mins at different temperatures are extracted in Fig. 5b from Fig. 5a. More tests (65, 70, 75 °C for 360 mins and 75 °C for 60 mins) are conducted to confirm the wear trend in the temperature range of 60~80 °C (see the dash lines in Fig. 5b). For the tests at 60 mins and 360 mins, the maximum wear occurs at 80 °C and 75 °C, respectively. It is speculated that the change of the wear mechanism of FFO may happen around 75/80 °C. As the difference between the two temperatures is minor, to simplify the description, the subsequent description uses 80 °C as the threshold to divide the wear trend of FFO. Hence, it can be summarised that the wear trend when using FFO is two-phase temperature-dependent, that is, phase (I): in the low-temperature range of 60~80 °C, wear increases with the increase in temperature; and phase (II): in the high-temperature range of 80~120 °C, when the temperature rises, the wear decreases.

Considering the viscosity of the lubricants decreases with increasing temperature, the lower wear at 60 °C may be because it is not entirely in the boundary lubrication regime, so the fluid carries part of the applied load between asperities, resulting in the reduction of wear and tribofilm formation. To further investigate the effect of this factor, the author conducted a set of experiments with a lower λ ratio by only reducing entrainment speed from 0.1 m/s to 0.01 m/s. The wear results at a lower λ ratio still exhibit the same two-phase trend with temperature (results are shown in Supplementary Material for brevity), so the influence of viscosity can be eliminated. Based on these results, it can be suggested that the change of wear mechanism as a function of testing temperature could be mainly caused by different chemical compositions or the formation process of the tribofilm in the wear track.

4 Chemical Analysis

4.1 Raman Analysis

Since FFO contains ZDDP and overbased calcium sulphonate detergent, it is speculated that phosphate and sulphide are mainly present in the tribofilm. Raman spectroscopy is used for analysis, in which the Raman shift ranges of 200~500 cm^{-1} and 800~1200 cm^{-1} are selected as the spectral analysis sections for sulphide [53-59] and phosphate [60-62], respectively.

Fig. 6(a~d) shows the sulphide sections for the tribofilm after 3 hours of testing at different temperatures. The possible sulphides in tribofilm are likely to be FeS/FeS_2, ZnS, and CaS. At all tested temperatures, the Raman spectra are mainly composed of a strong peak at 374±2 cm^{-1} accompanied by a small peak at 337±3 cm^{-1} and a weak peak at 418±3 cm^{-1}, which are consistent with the reference spectra of pyrite-FeS_2 [53]. In addition, the weak peaks at 319 cm^{-1} and 315 cm^{-1} appear at 100 °C and 120 °C, respectively, which may be attributed to the marcasite structure of FeS_2 [54]. When the temperature increases, iron sulphide's signal intensity significantly reduces. However, the typical peak for ZnS is around 349 cm^{-1} [55, 56], which cannot be separated from the Raman results. Furthermore, the primary Raman shifts for Ca-S at 285 cm^{-1}, 215 cm^{-1}, 185 cm^{-1}, and 160 cm^{-1} [57] are not found within the measurement range of the Raman analysis. Compared to the Raman results for the ZDDP tribofilm in Ref.[58], the peaks detected for sulphides are likely to be 386 cm^{-1} for Fe-S and 351 cm^{-1} for Zn-S. However, for an engine oil containing ZDDP and calcium S-based detergent, the peak for FeS_2 was detected [59]. Thus, the iron sulphides detected in FFO tribofilm are mainly the product of interaction between ZDDP and detergent.

Fig. 6(e~h) shows the phosphate section for the tribofilm after testing for 3 hours at different temperatures. The possible phosphates in the tribofilm are probably Ca/Zn/Fe phosphate. There are mainly two strong peaks and one weak peak. The first peak is at 952±1cm^{-1}, which can be assigned to ν_1-PO_4 with the symmetrical stretching mode [61]. It is more likely to be assigned to calcium phosphate due to the presence of detergents, but there may be a small amount of zinc phosphate and/or iron phosphate. The second peak is at 1080±1 cm^{-1}, which can be assigned to ν_1-CO_3 with the symmetrical stretching mode or ν_3-PO_4 with the antisymmetric stretching mode [61, 62]. The latter has a lower Raman shift, and its signal intensity usually is not higher than the peak ν_1-PO_4. Therefore, it is mainly attributed to the presence of calcium carbonate when the temperature is lower than 100 °C. Between the two peaks, weak peaks at 997±2 cm^{-1} and 1041±4 cm^{-1} can be assigned to other stretching modes of P-O from PO_4 or PO_3 group [60-62].

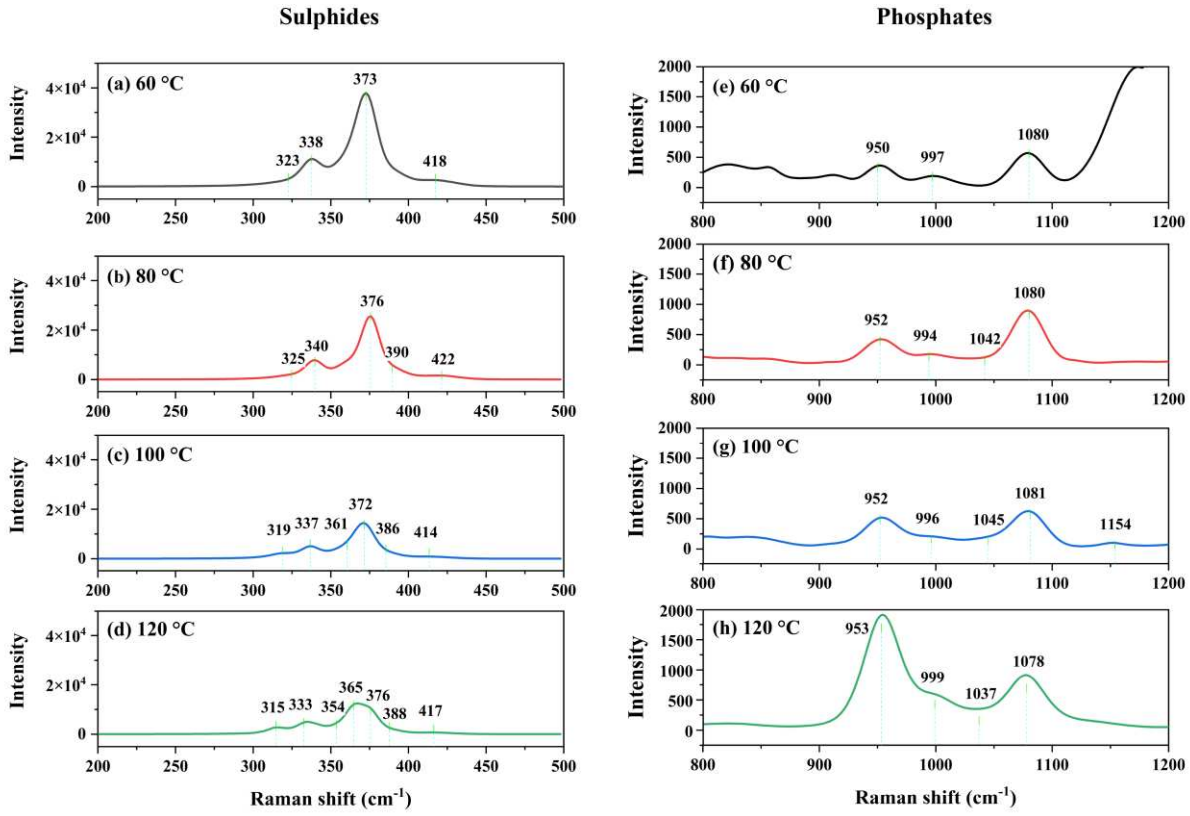

Fig. 6 Raman spectra of sulphide (a-d) and phosphate (e-h) in the tribofilms after testing for 3 hours at different temperatures (a,e) 60 °C, (b,f) 80 °C, (c,g) 100 °C, and (d,h) 120 °C.

It can be inferred from Raman analysis that the FFO tribofilm contains iron sulphide, calcium phosphate, and calcium carbonate. With the increase in temperature, the peak intensity of iron sulphide decreases, but that of phosphate increases.

4.2 XPS Depth Profiling Analysis

XPS depth profiling analysis combined with high-resolution elemental spectra is used to determine the chemical compositions of FFO tribofilm along the depth direction at different temperatures. The elements C, O, N, P, S, Ca, Fe, and Zn, are chosen for analysis. Since there is no N signal for all tested samples, N spectra are ignored. The XPS signals of C1s, O1s, P2p, S2p, Ca2p, and Zn2p3 at four temperatures are shown in Fig. 7 ~ Fig. 12, respectively.

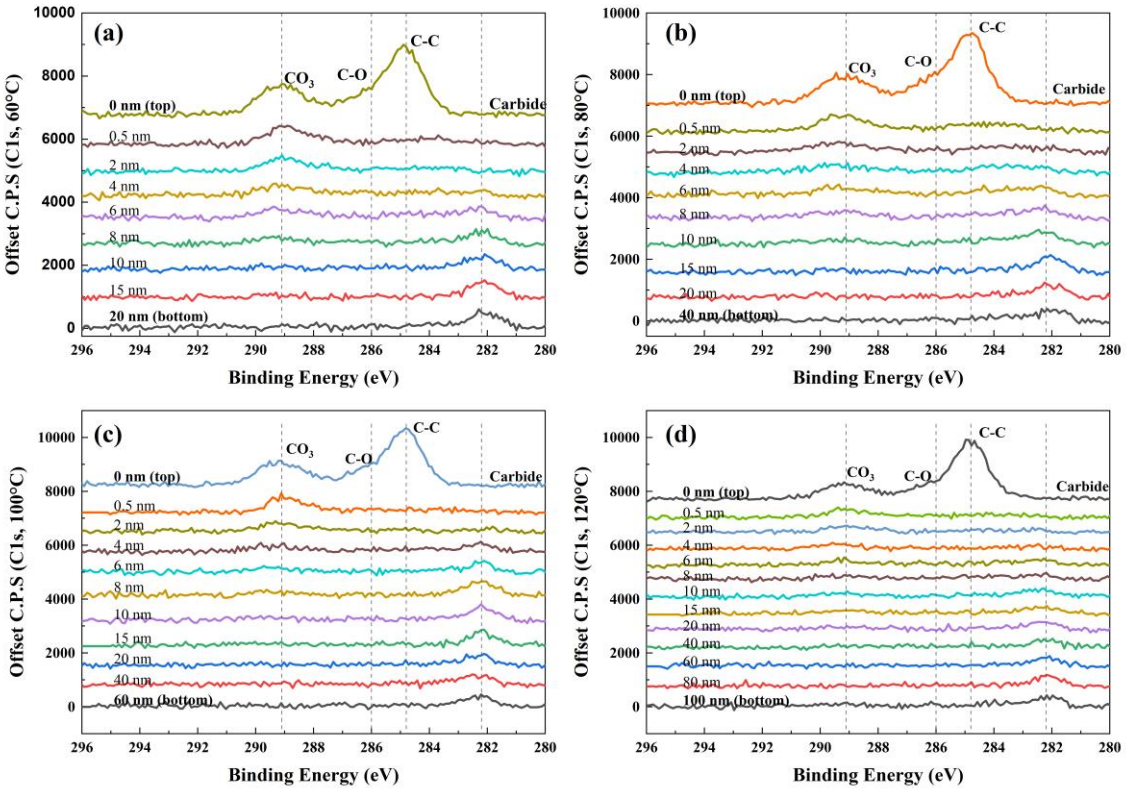

Fig. 7 The C1s spectra of XPS depth profiling of tribofilm on the disc after the 3-hour test at different temperatures (a) 60 °C, (b) 80 °C, (c)100 °C, and (d) 120 °C.

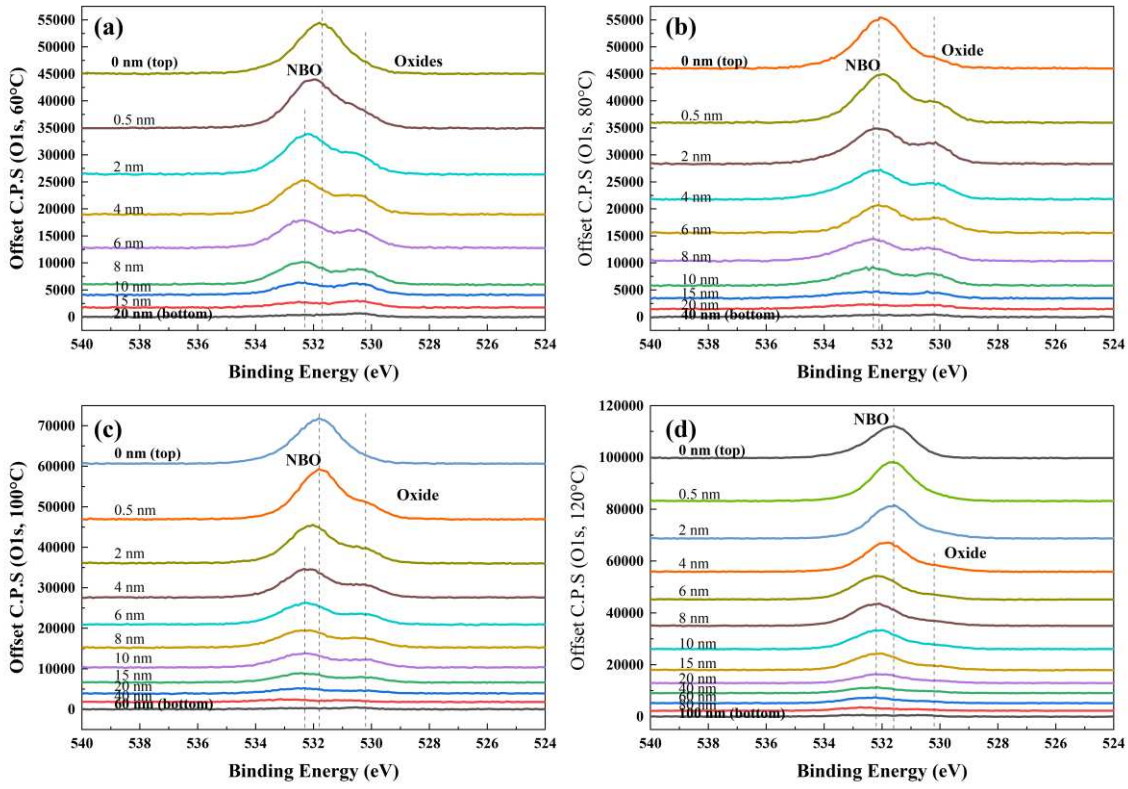

Fig. 8 The O1s spectra of XPS depth profiling of tribofilm on the disc after the 3-hour test at different temperatures (a) 60 °C, (b) 80 °C, (c)100 °C, and (d) 120 °C.

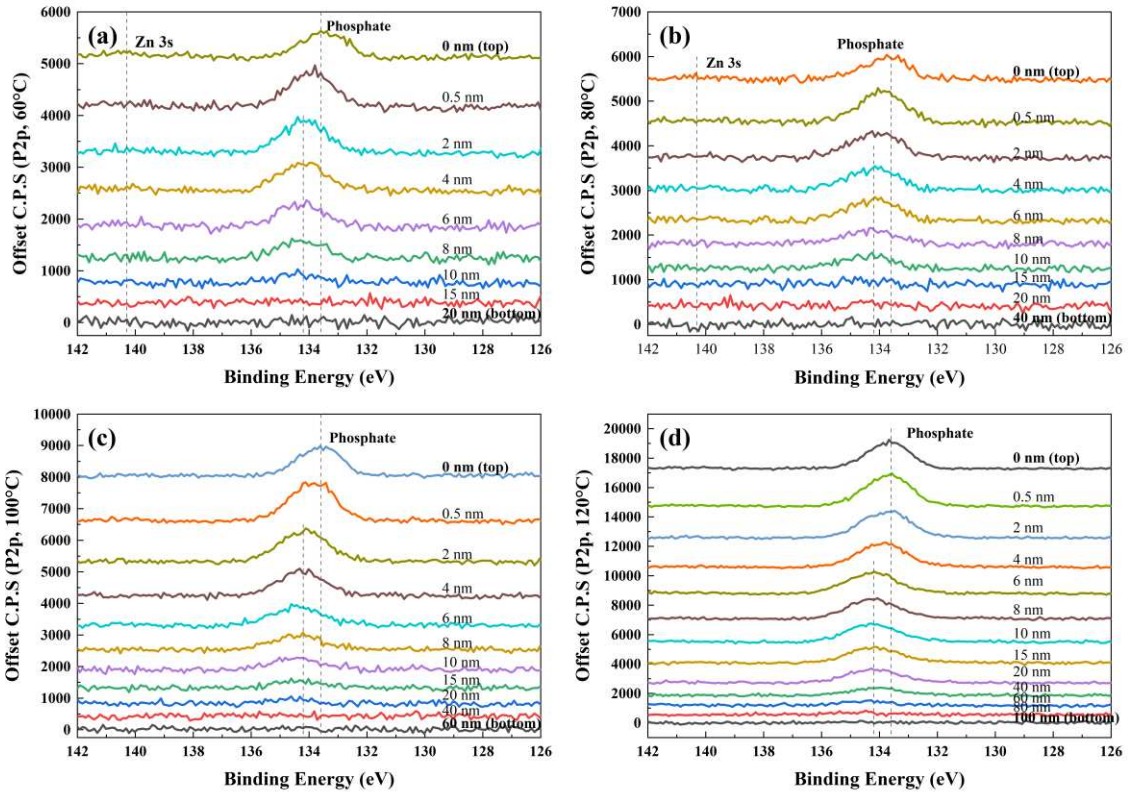

Fig. 9 The P2p spectra of XPS depth profiling of tribofilm on the disc after the 3-hour test at different temperatures (a) 60 °C, (b) 80 °C, (c)100 °C, and (d) 120 °C.

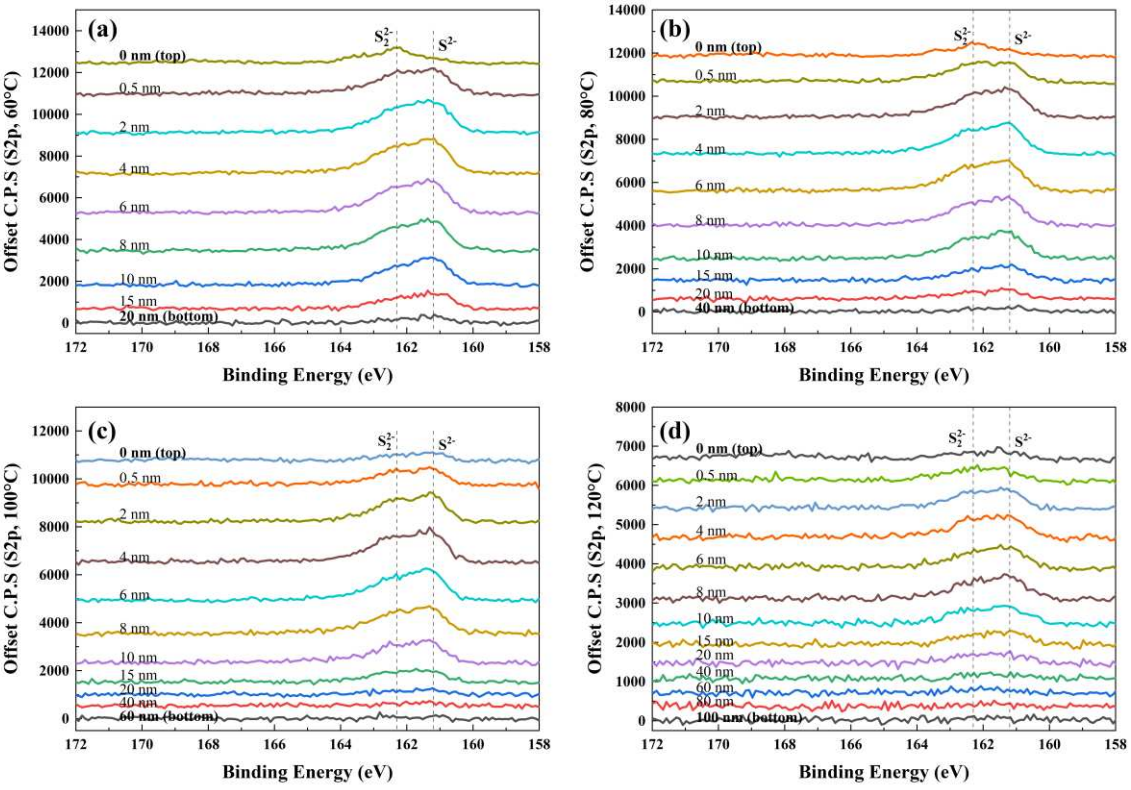

Fig. 10 The S2p spectra of XPS depth profiling of tribofilm on the disc after the 3-hour test at different temperatures (a) 60 °C, (b) 80 °C, (c)100 °C, and (d) 120 °C.

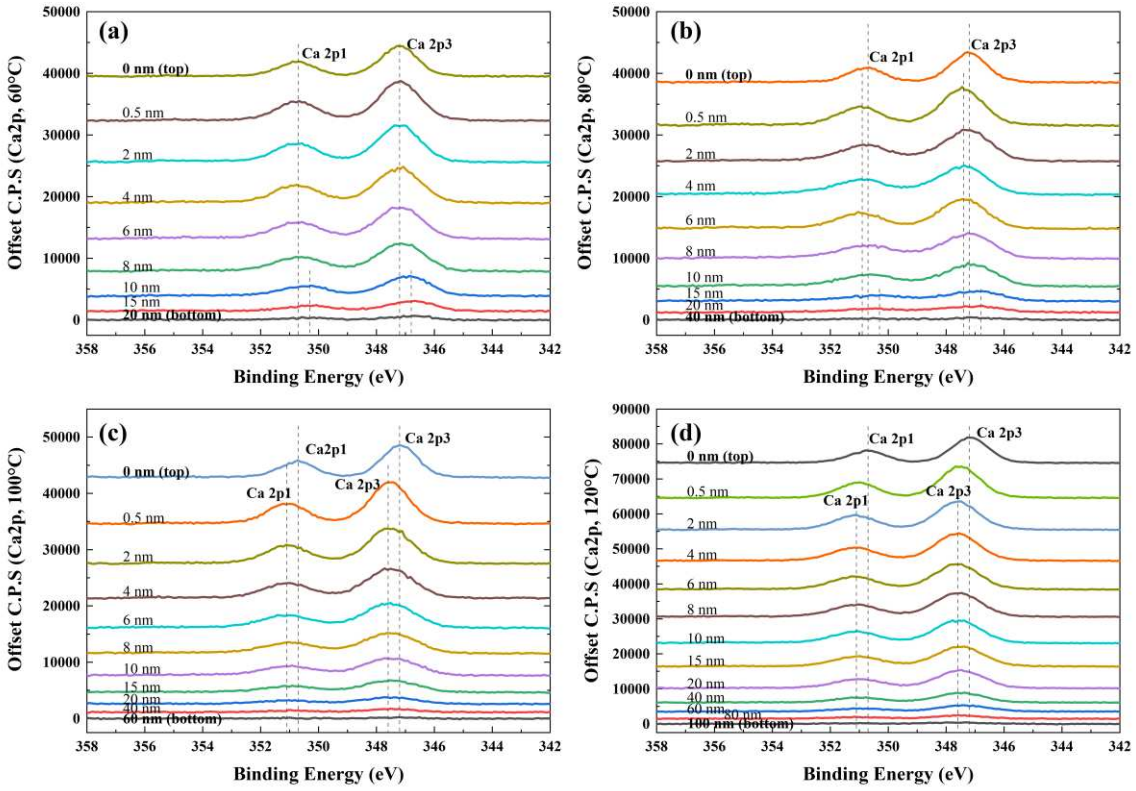

Fig. 11 The Ca2p spectra of XPS depth profiling of tribofilm on the disc after the 3-hour test at different temperatures (a) 60 °C, (b) 80 °C, (c)100 °C, and (d) 120 °C.

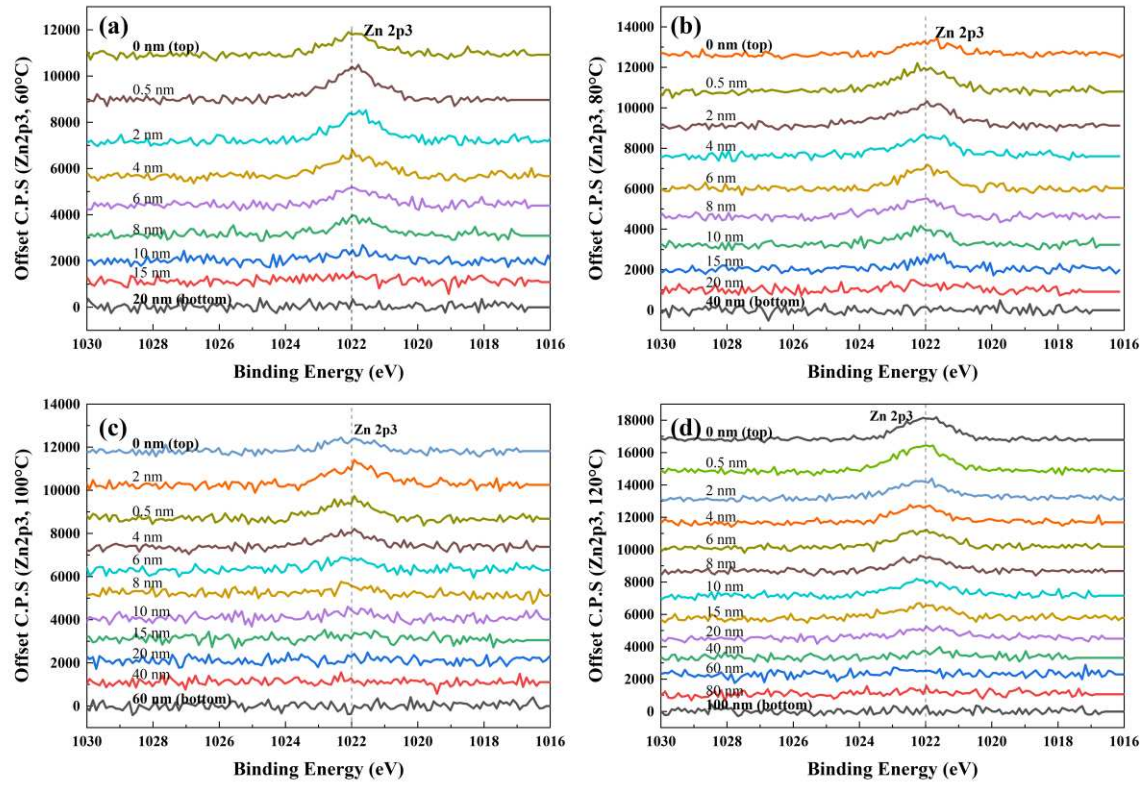

Fig. 12 The Zn2p3 spectra of XPS depth profiling of tribofilm on the disc after the 3-hour test at different temperatures (a) 60 °C, (b) 80 °C, (c)100 °C, and (d) 120 °C

Fig. 7 shows the variation of the C1s spectra with etching depths at four temperatures. Two separate peaks can be observed on the surface, 284.8 eV and 289.1 eV, which are attributed to the organic carbon bond (C-C, C-H) and the carbonate (CO_3) in calcium carbonate [6, 63, 64], respectively. Another peak hidden at 286 eV is the C-O bond in carbonate [65]. With the increased etching depth, another peak at 282.2 eV appeared, which may be assigned to the peak of carbide [66, 67], indicating that the depth reached the substrate.

The O1s spectra in Fig. 8 show the two prominent peaks at 530.2 eV and 531.7 eV, assigned to metal oxide [63] and NBO (non-bridging oxygen) in phosphate, carbonate, or sulphate [6, 63-65, 68], respectively. As the temperature increases, the peak intensity of the metal oxide decreases, indicating that there is more tribofilm formed on the surface, which is consistent with the experimental results of tribofilm thickness. The NBO peak moves to 532.1 eV in the middle layer of the tribofilm. These results may be due to an overlap with a BO (bridging oxygen, such as P-O-P) peak, which has higher binding energy than the NBO peak [45, 63].

The P2p spectra at different temperatures are shown in Fig. 9. Using an area ratio of 2:1 to split the peak due to the splitting of the 2p orbital, the binding energy of the P2p3 peak is approximately 133.2~133.8eV, which is attributed to the phosphate. On the surface of the tribofilm, the binding energy of this peak is lower, and as the etching depth increases, the peak shifts to the higher binding energy. The increase in the binding energy of the P2p3 (phosphate) peak may be due to the change in metal cations such as Ca^{2+}, Zn^{2+} and Fe^{2+} (the order of binding energy: $Ca^{2+} \leq Zn^{2+} < Fe^{2+}$) [6, 63, 68-73] or in the degree of phosphate polymerisation (the order of binding energy: Ortho< Pyro< Poly-phosphate) [74]. Therefore, the most likely phosphates can be calcium phosphate or short-chain zinc phosphate. In addition, the Zn3s peak with a binding energy of 140.3 eV can be fitted, indicating zinc phosphate's presence. However, it only appears on the surface of tribofilm and under lower temperature conditions (marked in Fig. 9a and b).

Fig. 10 shows the S2p spectra at different temperatures where two peaks are marked. The one with a lower binding energy of 161.7 eV is derived from mono-sulphides, while the other peak at 162.3±0.1 eV is attributed to disulphide [63, 75, 76]. Raman analysis indicates the existence of iron disulphide in the FFO tribofilm, which is consistent with the XPS results. In the further peak fitting of each spectrum, there is a weak peak around 168.2 eV on the top surface of the tribofilm (not shown in Fig. 10). Such a peak is assigned to the sulphate group with less sulphonate [64, 77, 78], derived from over-based calcium sulphonate detergent.

As for Ca2p spectra in Fig. 11, two peaks, Ca2p3 and Ca2p1, appear that can be assigned to $CaSO_4/SO_3$, $CaCO_3$, $Ca(PO_4)_x$, and CaS. The first three can be inferred from the S2p, C1s, and P2p spectra, respectively, but there is no signal in both XPS and Raman spectra showing the existence of CaS. The detailed binding energy at each temperature will be discussed later. The Zn2p3 peak in Fig. 12 has the binding energy of 1022±0.2 eV, attributed to zinc phosphate [63, 70], and it only presents in the upper part of the tribofilm.

The XPS analysis of the elemental spectra illustrates that the chemical compositions of FFO tribofilm are similar at the four temperatures. The products in the depth direction are, starting from the surface, calcium carbonate/calcium sulphate, phosphate (mainly Ca), sulphide (FeS_2), and iron oxide/substrate. To further analyse the differences in each composition at different temperatures and its effect on the wear mechanism, the area and the binding energy of prominent peaks as a function of etching depth at different temperatures are compared, as shown in Fig. 13.

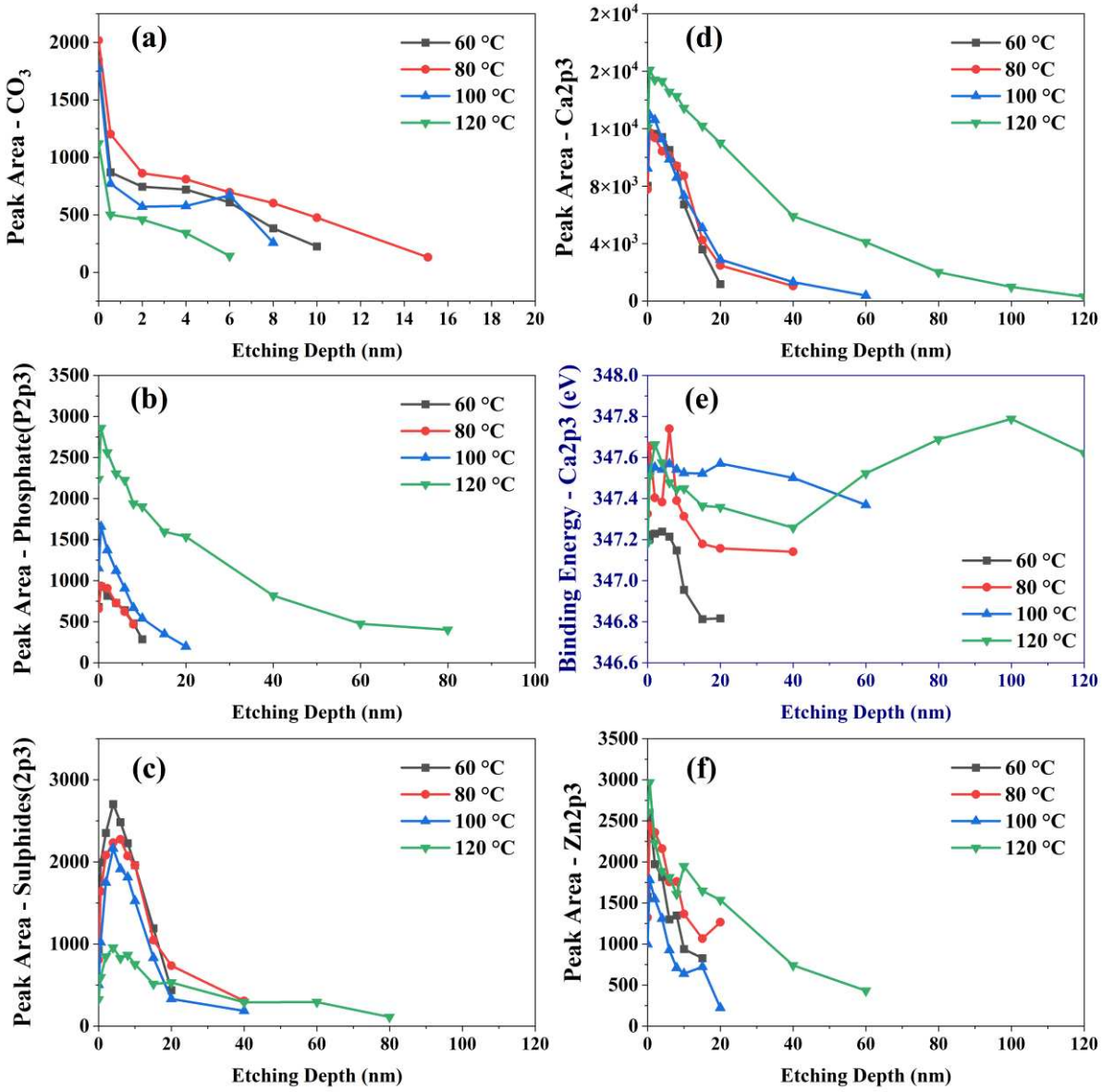

Fig. 13 The peak areas or the binding energy of the main peaks to identify the chemical compositions of the FFO tribofilm are extracted from the XPS depth profiling analysis to compare the differences at different temperatures. ((a) peak area of carbonate - C1s spectra, (b) peak area of phosphate (P 2p3) - P2p spectra, (c) peak area of sulphides (S 2p3 and S_2 2p3) - S2p spectra, (d) peak area of Ca2p3 - Ca2p spectra, (e) binding energy of Ca2p3 - Ca2p spectra and (f) peak area of Zn2p3 - Zn2p3 spectra.)

Calcium carbonate is the mineral core in the detergent. As shown in Fig. 13a, the maximum peak area of calcium carbonate appears at the top layer of the tribofilm at all temperatures but drops sharply at 0.5~2 nm from the surface. The calcium carbonate appears on the surface of the tribofilm, which is consistent with many studies on the tribofilm produced by the over-based calcium sulphonate detergent [6, 26]. By contrast, the peak area is highest at 80 °C, which seems to be similar to the wear trend. However, the author did the same tests at a lower λ ratio by changing the entrainment speed and did not find the exact correlation between calcium carbonate and wear (results are shown in Supplementary Material for brevity). Moreover, calcium carbonate may account for the antiwear property of detergents [27]. Therefore, although the influence of calcium carbonate on the wear trend cannot be excluded, it is difficult to use it alone to explain the wear mechanism.

Phosphate and sulphides should be the main compositions in the FFO tribofilm, so the peak areas of phosphate (P 2p) and sulphide (S 2p and S_2 2p) are analysed in Fig. 13b and c, respectively. At all four temperatures, the peak values of phosphate are at 0.5 nm near the surface and decrease gradually with the increase of depth (Fig. 13b). In contrast, the peak area of phosphate is almost unchanged from 60 °C to 80 °C (Phase (I) of the wear trend), whereas it increases significantly from 80°C to 120 °C (Phase (II) of the wear trend). Especially at 120 °C, the peak area and depth of phosphate have a significant increase. However, the peak area of sulphide at different temperatures shows an opposite trend to that of phosphate (see Fig. 13c), which is consistent with the Raman results. The peak area of sulphides decreases slightly from 60 °C to 100 °C. Then, there is a significant reduction from 100 °C to 120 °C. At the four temperatures, with the increased etching depth, the peak area sulphides increase rapidly from the beginning to the depth of 2 nm, reaching the maximum value, which is deeper than the peak depth of phosphate. It may indicate that part of the sulphide is covered by phosphate, which is similar to the chemical structure of the ZDDP tribofilm [14].

The Ca ion is provided only by detergents, reflecting its involvement in the tribofilm formation. At all temperature, the areas of the Ca2p3 peak decreases with the increase of depth (see Fig. 13d). At 120 °C, the peak area has the highest value. Since there are many types of calcium-containing compounds and their corresponding binding energies of Ca2p3 peaks are different, the binding energies of Ca2p3 peaks in the etching depth direction at different temperatures are further compared (see Fig. 13e). The binding energy at 60 °C is lower than those at the other temperatures, although the peak area at 60 °C is quite similar to those at 80 °C and 100 °C. This indicates that detergents participate in tribofilm formation at 60 °C to a similar extent to that at 80 °C/100 °C. However, less calcium phosphate is produced in the tribofilm at 60 °C. Therefore, it can be speculated that the antiwear properties of detergents themselves play a leading role in reducing wear at 60 °C, rather than the antiwear mechanism of the phosphates. In the range of 80~120 °C, the binding energy of the peak fluctuates between 347.4 eV and 347.7 eV at a thickness of 10 nm on the tribofilm surface, indicating the presence of calcium carbonate [64, 65, 78] and calcium sulphate [65, 77-79] on the surface. Then, the binding energy of the main part of the tribofilm is around 347.4 eV, which is attributed to calcium phosphate [68]. In addition, the binding energy increases near the substrate at 120 °C, which may also be attributed to the calcium

phosphate with higher binding energy, or from the error caused by the decrease of spectral signal when it approaches the substrate.

The other cation Zn is derived only from ZDDP. The peak areas of Zn2p3 representing zinc phosphate in the tribofilm at different temperatures are compared, as shown in Fig. 13f. It mainly exists on the surface of the tribofilm, which may be the chemisorption of ZDDP decomposition products or the intermediate product in the reaction of forming calcium phosphate. This process should occur mostly at 120 °C because the peak area of Zn2p3 has the most significant depth and the maximum value.

5 Discussions

5.1 Possible Wear Mechanisms

In this work, wear is the loss of substrate material during the rubbing, that is, the iron loss. It may mainly originate from direct contact between the two surfaces when the tribofilm is insufficient to cover the surface (mechanical wear) or be consumed in the tribochemical reactions between the surface and the additives to form the tribofilm (tribochemical wear). The wear results of FFO show that the wear rate is almost unchanged during the first 5 mins. In addition, the surface is relatively smooth, so the temperature-dependent iron loss due to mechanical wear can be ignored. Therefore, the wear mechanism of FFO mainly comes from the difference in the tribochemical wear pathway at different temperatures.

The chemical analysis of FFO tribofilm indicates that the most temperature-dependent compositions in the tribofilm are phosphates and sulphides. As the temperature increases, the signal intensity of the phosphate in tribofilm increases, while that of the iron sulphide decreases (see Fig. 6, Fig. 13b, and c). However, almost no composition can directly explain FFO's two-phase temperature-dependent wear mechanism. This indicates that the wear mechanism is not only related to the chemical composition of the reaction product (tribofilm) but also related to its formation process.

It can be seen from XPS analysis that the additives ZDDP and overbased calcium sulphonate detergent are the most involved in the formation of the FFO tribofilm. Many previous studies on the two additives have shown a competitive relationship. The primary phenomenon is that the overbased calcium sulphonate will reduce the antiwear performance of ZDDP because the Ca ion will replace the cation in zinc phosphate to form calcium phosphate [25-27]. This is also consistent with the significant phosphate detected in the FFO tribofilm. The higher amount of calcium phosphate in the FFO tribofilm at higher temperatures is the main factor in reducing wear in the Wear Phase (II).

In contrast, the wear reduction at lower temperatures in the Wear Phase (I) is thought to be dominated by the antiwear performance of the detergent itself, that is, by sulphides and calcium carbonate. The higher wear results between the two Phases are likely due to the antagonism of the two additives. This indicates that although the

wear behaviour of FFO depends on the competitive relationship between the two additives, the dominant antiwear tribofilm could change as a function of temperature, resulting in different levels of iron loss. Thus, three mechanisms are proposed to explain the wear mechanism of FFO at different temperatures, as shown in Fig. 14.

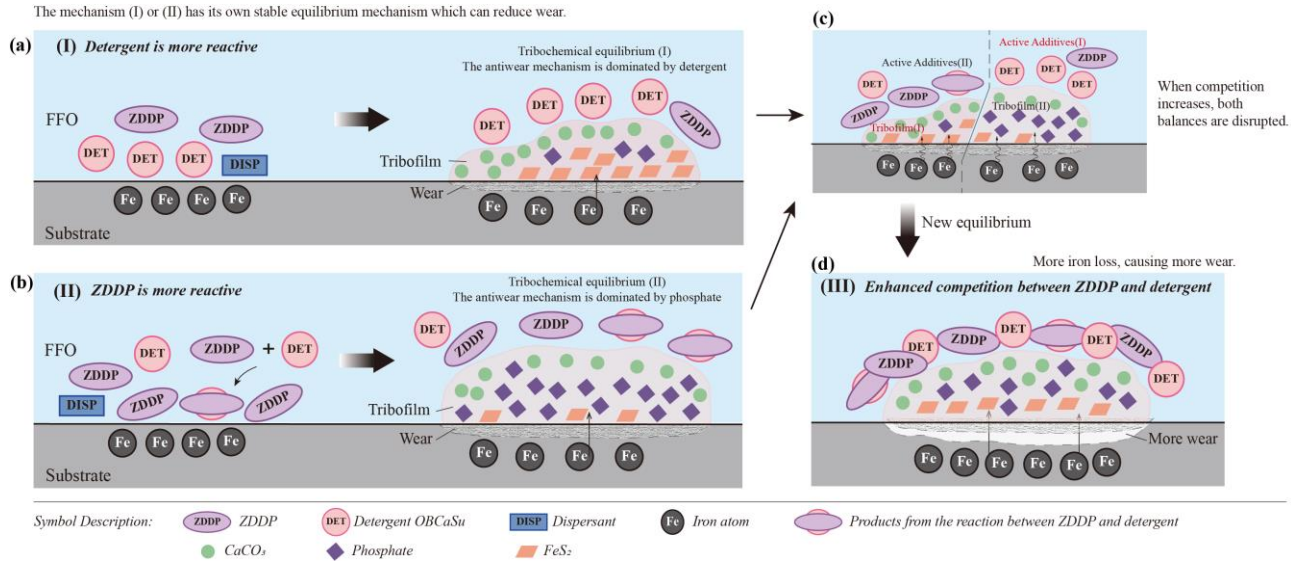

Fig. 14 Three mechanisms to explain FFO's wear mechanism at different temperatures. (a) is the Mechanism (I) when detergent is more reactive; (b) is the Mechanism (II) when ZDDP is more reactive; (c) and (d) are the Mechanism (III) when the competition is enhanced between ZDDP and detergent.

- Mechanism (I) The reactivity of detergent is greater than that of ZDDP

Suppose detergent preferentially reacts with the iron surface to form a boundary film of crystalline $CaCO_3$ or CaO. In this case, it can prevent or reduce the reaction of ZDDP with the substrate (see Fig. 14a). This can happen at low temperatures because the reaction activity of ZDDP with the substrate is weak. In this case, it seems to be less iron consumption in this tribochemical path because the generation of boundary film hardly needs the participation of iron [15]. Therefore, the iron may be lost by forming iron sulphide or by direct contact due to inadequate protection by the tribofilm. Iron sulphides have been reported to increase the lubricity of the surface [51, 52] and can reduce abrasion to a certain extent [80-82]. In addition, calcite ($CaCO_3$) film has a certain degree of resistance to wear [5, 20, 23, 28, 83]. This may be why although the tribofilm thickness is the lowest at 60 °C, the wear volume is still low.

- Mechanism (II) ZDDP is more reactive than detergent

For ZDDP, phosphate has antiwear properties under mild wear conditions [9]. The chemical analysis of FFO tribofilm shows that the peak assigned to phosphate at 120 °C has a higher signal intensity than that at 100 °C. In Phase (II) of the wear mechanism, wear decreases with increasing temperature. This also reflects the wear resistance of phosphate, although it is the calcium phosphate mainly present in FFO tribofilm rather than zinc phosphate. Kasrai *et al.* proposed two possible reaction paths for the formation of calcium phosphate by ZDDP

and calcium detergent: (1) ZDDP decomposes and then reacts with Ca^{2+}; and (2) polyphosphate produced by ZDDP, decomposes and reacts to form calcium phosphate [27]. Therefore, in the higher temperature range, when ZDDP is more reactive than the detergent, the antiwear property of phosphate plays a dominant role in reducing wear. In this way, the iron in the substrate is consumed by tribochemical reactions to supplement the tribofilm removed during the rubbing process, as shown in Fig. 14b.

- Mechanism (III) Strong competition between ZDDP and detergents

Mechanisms (I) and (II) reflect the detergent's and ZDDP's advantages in reducing wear, respectively. However, suppose that both additives are highly reactive. As shown in Fig. 14c, when the competition is enhanced, the tribofilm formed in Mechanism (I) faces the active additive environment in Mechanism (II) or the reverse, disrupting the chemical equilibrium, so the antiwear property of either of them cannot perform well. Then, the unstable tribofilm forms at the beginning and increases friction, causing higher wear. Finally, it will achieve a new equilibrium (see Fig. 14d). This may explain why there is a 'growth - reduction - regrowth' process for the growth rate of the tribofilm at 80 °C and 100 °C. Moreover, the wear and the initial friction coefficient are higher at both temperatures. Although this process is difficult to represent in terms of specific chemical reaction formula, it can be inferred that the path of iron loss is still related to the consumption in the tribochemical reaction of the tribofilm formation.

As for the mild wear mechanism when using FFO on the steel surface, the iron content in tribofilm can directly reflect the consumption of the steel substrate (iron loss) in tribochemical reaction, and it is also a way to unify the above three possible mechanisms. This provides an experimental basis for developing a wear model involving the tribochemistry of FFO.

5.2 Effect of Dispersant

Dispersants can form complexes with ZDDP molecules [8, 30-32] and affect the contact between ZDDP and metal surfaces [33-35]. Suppose the dispersant is involved in tribofilm formation, specifical succinimide in this study. In this case, the N atom should be detected in tribofilm [84], but there is no N signal from the depth profile analysis of XPS. Therefore, the influence of the dispersant on the composition of tribofilm appears to be minimal. However, the dispersant was reported to increase the decomposition temperature of ZDDP [20]. Martin *et al.* found that the dispersant can reduce the chemisorption of ZDDP and phosphate formation at 60 °C [85]. This could be why FFO tribofilm has the highest peak signal of phosphate at 120 °C and reduces wear. The corresponding antiwear mechanism when using FFO at this temperature is similar to ZDDP. This mechanism of reducing wear through phosphate appears to operate at higher temperatures in the FFO tested than in ZDDP-only lubricant.

6 Conclusions

This paper studied the wear mechanism for an FFO typically used in hydraulic piston pumps, which contains the antiwear additive ZDDP, detergents, and dispersant. Here are some findings summarised as follows.

Firstly, the growth of FFO tribofilm has a similar trend to the tribofilm formed by ZDDP alone in the base oil, including a growth phase and a stable phase. However, a two-phase temperature-dependent wear trend on the steel surfaces is exhibited when using FFO in the tested temperature range. That is, wear increases first (Phase I) and then decreases (Phase II) with the increase in tribofilm thickness/temperature.

Secondly, the wear mechanism for the FFO is related to the chemical composition and the formation process of the tribofilm. Both Raman and XPS analysis found that the most temperature-dependent compositions are phosphate and sulphide. As the temperature increases, the intensity of the phosphate peak increases, while that of the iron sulphide peak decreases.

Thirdly, a hypothesis of the mechanisms of priority reaction or enhanced competition between ZDDP and the overbased calcium sulphonate detergent is proposed to explain the wear characteristics for FFO from the perspective of iron consumption in the tribochemical reactions path. Specifically, the lower wear in Phase (I) and (II) is mainly attributed to the detergent's antiwear property and the phosphate-based antiwear mechanism provided by ZDDP, respectively. The higher wear between the two Phases is due to the increased antagonism between the two additives.

In further work, the FFO's experimental data and wear mechanism will be applied to develop the wear model in Part (II) of this series of papers.

References

1. Holmberg, K. and A. Erdemir, *Influence of tribology on global energy consumption, costs and emissions.* Friction, 2017. **5**(3): p. 263-284.

2. Holmberg, K., et al., *Global energy consumption due to friction and wear in the mining industry.* Tribology International, 2017. **115**: p. 116-139.

3. Givens, W., et al., *Hydraulic fluids.* Fuels and Lubricants Handbook, 2003.

4. Costello, M.T., *Study of Surface Films of Amorphous and Crystalline Overbased Calcium Sulfonate by XPS and AES.* Tribology Transactions, 2006. **49**(4): p. 592-597.

5. Najman, M., et al., *Combination of ashless antiwear additives with metallic detergents: interactions with neutral and overbased calcium sulfonates.* Tribology International, 2006. **39**(4): p. 342-355.

6. Costello, M.T. and R.A. Urrego, *Study of Surface Films of the ZDDP and the MoDTC with Crystalline and Amorphous Overbased Calcium Sulfonates by XPS.* Tribology Transactions, 2007. **50**(2): p. 217-226.

7. Yin, Z., et al., *Application of soft X-ray absorption spectroscopy in chemical characterization of antiwear films generated by ZDDP Part II: the effect of detergents and dispersants.* Wear, 1997. **202**(2): p. 192-201.

8. Zhang, J., E. Yamaguchi, and H. Spikes, *The antagonism between succinimide dispersants and a secondary zinc dialkyl dithiophosphate.* Tribology Transactions, 2014. **57**(1): p. 57-65.

9. Sakamoto, T., et al., *The reaction layer formed on steel by additives based on sulphur and phosphorus compounds under conditions of boundary lubrication.* Wear, 1982. **77**(2): p. 139-157.

10. Fujita, H. and H. Spikes, *The formation of zinc dithiophosphate antiwear films.* Proceedings of the Institution of Mechanical Engineers, Part J: Journal of Engineering Tribology, 2004. **218**(4): p. 265-278.

11. Taylor, L., A. Dratva, and H.A. Spikes, *Friction and Wear Behavior of Zinc Dialkyldithiophosphate Additive.* Tribology Transactions, 2000. **43**(3): p. 469-479.

12. Fujita, H., R. Glovnea, and H. Spikes, *Study of zinc dialkydithiophosphate antiwear film formation and removal processes, part I: experimental.* Tribology transactions, 2005. **48**(4): p. 558-566.

13. Fuller, M.S., et al., *The use of X□ray absorption spectroscopy for monitoring the thickness of antiwear films from ZDDP.* Tribology Letters, 2000. **8**(4): p. 187-192.

14. Spikes, H., *The history and mechanisms of ZDDP.* Tribology letters, 2004. **17**(3): p. 469-489.

15. Mansot, J., M. Hallouis, and J. Martin, *Colloidal antiwear additives 2. Tribological behaviour of colloidal additives in mild wear regime.* Colloids and Surfaces A: Physicochemical and Engineering Aspects, 1993. **75**: p. 25-31.

16. Giasson, S., et al., *Study of boundary film formation with overbased calcium sulfonate by PM-IRRAS spectroscopy.* Thin Solid Films, 1994. **252**(2): p. 111-119.

17. Cizaire, L., et al., *Tribochemistry of overbased calcium detergents studied by ToF-SIMS and other surface analyses.* Tribology Letters, 2004. **17**(4): p. 715-721.

18. Costello, M.T., R.A. Urrego, and M. Kasrai, *Study of surface films of crystalline and amorphous overbased sulfonates and sulfurized olefins by X-ray absorption near edge structure (XANES) spectroscopy.* Tribology Letters, 2007. **26**(2): p. 173-180.

19. Topolovec-Miklozic, K., T.R. Forbus, and H. Spikes, *Film Forming and Friction Properties of Overbased Calcium Sulphonate Detergents.* Tribology Letters, 2008. **29**(1): p. 33-44.

20. Shirahama, S. and M. Hirata, *The effects of engine oil additives on valve train wear.* Lubrication Science, 1989. **1**(4): p. 365-384.

21. Delfort, B., M. Born, and B. Daoudal, *Functionalization of overbased calcium sulfonates-synthesis and evaluation of antiwear and extreme-pressure performances.* Lubrication Engineering, 1995: p. Medium: X; Size: pp. 981-990.

22. Delfort, B., B. Daoudal, and L. Barré, *Particle size determination of (functionalized) colloidal calcium carbonate by small angle x-ray scattering—Relation with antiwear properties.* Tribology transactions, 1999. **42**(2): p. 296-302.

23. Minami, I., et al., *Tribochemical approach toward mechanism for synergism of lubricant additives on antiwear and friction reducing properties*, in *Tribology and Interface Engineering Series*, D. Dowson, et al., Editors. 2005, Elsevier. p. 259-268.

24. Willermet, P., et al., *Formation, structure, and properties of lubricant□derived antiwear films.* Lubrication Science, 1997. **9**(4): p. 325-348.

25. Kasrai, M., et al., *Study of the effects of Ca sulfonate on antiwear film formation by X-ray absorption spectroscopy using synchrotron radiation.* Journal of synchrotron radiation, 1999. **6**(3): p. 719-721.

26. Wan, Y., et al., *Effects of detergent on the chemistry of tribofilms from ZDDP: studied by X-ray absorption spectroscopy and XPS*, in *Tribology series*. 2002, Elsevier. p. 155-166.

27. Kasrai, M., et al., *X-Ray Absorption Study of the Effect of Calcium Sulfonate on Antiwear Film Formation Generated From Neutral and Basic ZDDPs: Part 1—Phosphorus Species.* Tribology Transactions, 2003. **46**(4): p. 534-542.

28. Kasrai, M., et al., *X-Ray Absorption Study of the Effect of Calcium Sulfonate on Antiwear Film Formation Generated From Neutral and Basic ZDDPs: Part 2 — Sulfur Species.* Tribology Transactions, 2003. **46**(4): p. 543-549.

29. Booth, J.E., *The feasibility of using electrostatic charge condition monitoring for lubricant additive screening*, *University of Southampton*. 2008.

30. Gallopoulos, N.E. and C.K. Murphy, *Interactions between a zinc dialkylphosphorodithioate and lubricating oil dispersants.* ASLE TRANSACTIONS, 1971. **14**(1): p. 1-7.

31. Inoue, K. and H. Watanabe, *Interactions of engine oil additives.* ASLE transactions, 1983. **26**(2): p. 189-199.

32. Shiomi, M., et al., *Interaction between zinc dialkyldithiophosphate and amine.* Lubrication Science, 1989. **1**(2): p. 131-147.

33. Rounds, F., *Changes in friction and wear performance caused by interactions among lubricant additives.* Lubrication Science, 1989. **1**(4): p. 333-363.

34. Zhang, Z., et al., *Study of the Interaction of ZDDP and Dispersants Using X-ray Absorption Near Edge Structure Spectroscopy—Part 1: Thermal Chemical Reactions.* Tribology Letters, 2003. **15**(4): p. 377-384.

35. Plaza, S., *The Effect of Other Lubricating Oil Additives on the Adsorption of Zinc Di-Isobutyldithiophosphate on Fe and γ-Fe2O3 Powders.* ASLE transactions, 1987. **30**(2): p. 241-247.

36. Kosarieh, S., et al., *Tribological performance and tribochemical processes in a DLC/steel system when lubricated in a fully formulated oil and base oil.* Surface and Coatings Technology, 2013. **217**: p. 1-12.

37. Aota, H., et al., *Tribological Properties of Nitrided Steels Lubricated with Fully Formulated Oils in Boundary Lubrication Condition.* Tribology Online, 2018. **13**(3): p. 166-171.

38. Pereira, G., et al., *Chemical and mechanical analysis of tribofilms from fully formulated oils Part 1 – Films on 52100 steel.* Tribology - Materials, Surfaces & Interfaces, 2013. **1**(1): p. 48-61.

39. Wan, S., et al., *Tribochemistry of adaptive integrated interfaces at boundary lubricated contacts.* Sci Rep, 2017. **7**(1): p. 9935.

40. Taylor, L.J. and H. Spikes, *Friction-enhancing properties of ZDDP antiwear additive: part I—friction and morphology of ZDDP reaction films.* Tribology transactions, 2003. **46**(3): p. 303-309.

41. Topolovec-Miklozic, K., T.R. Forbus, and H.A. Spikes, *Film thickness and roughness of ZDDP antiwear films.* Tribology Letters, 2007. **26**(2): p. 161-171.

42. Shimizu, Y. and H.A. Spikes, *The influence of slide–roll ratio on ZDDP tribofilm formation.* Tribology Letters, 2016. **64**(2): p. 19.

43. Ghanbarzadeh, A., et al., *A semi-deterministic wear model considering the effect of zinc dialkyl dithiophosphate tribofilm.* Tribology Letters, 2016. **61**(1): p. 12.

44. Ghanbarzadeh, A., et al., *Development of a new mechano-chemical model in boundary lubrication.* Tribology International, 2016. **93**: p. 573-582.

45. Ueda, M., A. Kadiric, and H. Spikes, *On the Crystallinity and Durability of ZDDP Tribofilm.* Tribology Letters, 2019. **67**(4).

46. Ueda, M., H. Spikes, and A. Kadiric, *In-situ observations of the effect of the ZDDP tribofilm growth on micropitting.* Tribology International, 2019. **138**: p. 342-352.

47. ISO, *6743-4:2015 Lubricants, industrial oils and related products (class L) — Classification — Part 4: Family H (Hydraulic systems)*. 2015, British Standars Insititution.

48. Totten, G.E. and V.J. De Negri, *Handbook of hydraulic fluid technology, second edition*. 2ed ed. CRC Press. 2011.

49. Benedet, J., et al., *Spurious mild wear measurement using white light interference microscopy in the presence of antiwear films.* Tribology Transactions, 2009. **52**(6): p. 841-846.

50. Tripaldi, G., A. Vettor, and H. Spikes, *Friction behaviour of ZDDP films in the mixed, boundary/EHD regime.* SAE transactions, 1996: p. 1819-1830.

51. Peng, T., et al., *Solid FeS lubricant: a possible alternative to MoS2 for Cu–Fe-based friction materials.* International Journal of Minerals, Metallurgy, and Materials, 2017. **24**(11): p. 1278-1283.

52. Peng, T., et al., *Low-cost solid FeS lubricant as a possible alternative to MoS2 for producing Fe-based friction materials.* International Journal of Minerals, Metallurgy, and Materials, 2017. **24**(1): p. 115-121.

53. Song, C., et al., *Hydrothermal synthesis of iron pyrite (FeS2) as efficient counter electrodes for dye-sensitized solar cells*. Solar Energy, 2016. **133**: p. 429-436.

54. Lafuente, B., et al., *1. The power of databases: The RRUFF project*, in *Highlights in mineralogical crystallography*. 2015, De Gruyter (O). p. 1-30.

55. Liu, T., et al., *Enhanced Raman intensity in ZnS planar and channel waveguide structures via carbon ion implantation.* Optical Materials, 2021. **112**: p. 110733.

56. Kim, J.H., et al., *Raman spectroscopy of ZnS nanostructures.* Journal of Raman Spectroscopy, 2012.

57. Avril, C., et al., *Raman spectroscopic properties and Raman identification of CaS-MgS-MnS-FeS-Cr2FeS4 sulfides in meteorites and reduced sulfur-rich systems.* Meteoritics & Planetary Science, 2013. **48**(8): p. 1415-1426.

58. Gachot, C., et al., *Microstructural and Chemical Characterization of the Tribolayer Formation in Highly Loaded Cylindrical Roller Thrust Bearings.* Lubricants, 2016. **4**(2): p. 19.

59. Faruck, A.A.M., et al., *How lubricant formulations and properties influence the performance of rotorcraft transmissions under loss of lubrication conditions.* Tribology International, 2020. **151**: p. 106390.

60. Brow, R.K., et al., *The short-range structure of zinc polyphosphate glass.* Journal of Non-Crystalline Solids, 1995. **191**(1-2): p. 45-55.

61. Kazanci, M., et al., *Complementary information on in vitro conversion of amorphous (precursor) calcium phosphate to hydroxyapatite from Raman microspectroscopy and wide-angle X-ray scattering.* Calcified tissue international, 2006. **79**(5): p. 354-359.

62. Berkani, S., et al., *Structural Changes in Tribo-Stressed Zinc Polyphosphates.* Tribology Letters, 2013. **51**(3): p. 489-498.

63. Heubergera, R. and A.R.a.N.D.S. , *XPS study of the influence of temperature on ZnDTP tribofilm composition.* 2007.

64. Cizaire, L., et al., *Chemical analysis of overbased calcium sulfonate detergents by coupling XPS, ToF-SIMS, XANES, and EFTEM.* Colloids and Surfaces A: Physicochemical and Engineering Aspects, 2004. **238**(1-3): p. 151-158.

65. Biesinger, M., *X-ray Photoelectron Spectroscopy (XPS) reference pages.* Surface Science Western, University of Western Ontario, Ontario, 2015.

66. Li, Y., et al., *Atomically Defined Iron Carbide Surface for Fischer–Tropsch Synthesis Catalysis.* ACS Catalysis, 2019. **9**(2): p. 1264-1273.

67. Furlan, A., et al., *Structure and bonding in amorphous iron carbide thin films.* Journal of Physics: Condensed Matter, 2015. **27**(4): p. 045002.

68. Chusuei, C.C., et al., *Calcium phosphate phase identification using XPS and time-of-flight cluster SIMS.* Analytical chemistry, 1999. **71**(1): p. 149-153.

69. Crobu, M., et al., *Tribochemistry of bulk zinc metaphosphate glasses.* Tribology letters, 2010. **39**(2): p. 121-134.

70. Minfray, C., et al., *A multi-technique approach of tribofilm characterisation.* Thin Solid Films, 2004. **447**: p. 272-277.

71. Wang, Y. and P.M. Sherwood, *Iron (III) phosphate (FePO4) by XPS.* Surface Science Spectra, 2002. **9**(1): p. 99-105.

72. Wang, Y., D.J. Asunskis, and P.M.A. Sherwood, *Iron (II) Phosphate (Fe3(PO4)2 by XPS.* Surface Science Spectra, 2002. **9**(1): p. 91-98.

73. Liu, Y., et al., *Synthesis of different structured FePO4 for the enhanced conversion of methyl cellulose to 5-hydroxymethylfurfural.* RSC Advances, 2017. **7**(81): p. 51281-51289.

74. Crobu, M., et al., *Chain-length-identification strategy in zinc polyphosphate glasses by means of XPS and ToF-SIMS.* Analytical and bioanalytical chemistry, 2012. **403**(5): p. 1415-1432.

75. Chaturvedi, S., et al., *XPS and LEED study of a single-crystal surface of pyrite.* American Mineralogist, 1996. **81**(1-2): p. 261-264.

76. Mattila, S., J. Leiro, and K. Laajalehto, *Surface XPS core-level shifts of FeS2.* Applied surface science, 2003. **212**: p. 97-100.

77. Bahadur, S., D. Gong, and J. Anderegg, *Investigation of the influence of CaS, CaO and CaF2 fillers on the transfer and wear of nylon by microscopy and XPS analysis.* Wear, 1996. **197**(1-2): p. 271-279.

78. Luque, A., et al., *Analysis of the surface of different marbles by X-ray photoelectron spectroscopy (XPS) to evaluate decay by SO 2 attack.* Environmental earth sciences, 2013. **68**(3): p. 833-845.

79. Nyenge, R.L., H.C. Swart, and O.M. Ntwaeaborwa, *Luminescent properties, intensity degradation and X-ray photoelectron spectroscopy analysis of CaS:Eu2+ powder.* Optical Materials, 2015. **40**: p. 68-75.

80. Wang, H.-D., et al., *Characterization and tribological properties of plasma sprayed FeS solid lubrication coatings.* Materials characterization, 2005. **55**(1): p. 43-49.

81. Wang, H.-d., et al., *Investigation on friction and wear behaviors of FeS films on L6 steel surface.* Applied Surface Science, 2005. **252**(4): p. 1084-1091.

82. Lee, I. and I. Park, *Solid lubrication coating of FeS layer on the surface of SKD 61 steel produced by plasma sulfnitriding.* Surface and Coatings Technology, 2006. **200**(11): p. 3540-3543.

83. Morizur, M. and O. Teysset, *Antiwear actions of additives in solid dispersion.* Lubrication Science, 1992. **4**(4): p. 277-299.

84. Yamaguchi, E.S., et al., *Study of the Interaction of ZDDP and Dispersants Using X-ray Absorption Near Edge Structure Spectroscopy—Part 2: Tribochemical Reactions.* Tribology Letters, 2003. **15**(4): p. 385-394.

85. Martin, J., et al., *Role of nitrogen in tribochemical interaction between Zndtp and succinimide in boundary lubrication.* Tribology International, 2000. **33**(7): p. 453-459.